A Tutorial and Overview of Retrospective Cost Adaptive Control

Yousaf Rahman[1], Antai Xie[1], Jesse B. Hoagg[2], and Dennis S. Bernstein[3]

CONTENTS

Abstract— The goal of this paper is to provide a tutorial on retrospective cost adaptive control (RCAC). RCAC is a discrete-time adaptive control technique that is applicable to stabilization, command following, and disturbance rejection. RCAC is based on the concept of retrospectively optimized control, where past controller coefficients used to generate past

[1]Graduate Student, Department of Aerospace Engineering, University of Michigan, 1320 Beal Ave., Ann Arbor MI 48109
[2]Assistant Professor, Department of Mechanical Engineering, University of Kentucky, 271 Ralph G. Anderson Building, Lexington KY 40506
[3]Professor, Department of Aerospace Engineering, University of Michigan, 1320 Beal Ave., Ann Arbor MI 48109

control inputs are re-optimized in the sense that if the re-optimized coefficients had been used over a previous window of operation, then the performance would have been better. Unlike signal processing applications such as estimation and identification, it is impossible to change past control inputs, and thus the re-optimized controller coefficients are used only to generate the next control input. This paper presents a tutorial on the algorithmic details of RCAC including the construction of the retrospective cost, the role of the target model, and the effect of tuning parameters. Numerical examples are given to illustrate each of these choices as well as the performance of RCAC for command following and disturbance rejection under minimal modeling of the plant dynamics and exogenous inputs. Properties of the closed-loop system are also compared to features of discrete-time, high-authority LQG controllers.

I. INTRODUCTION

A vast range of technological systems—from aerospace vehicles to chemical process plants to Segways—depend on feedback control. These applications typically rely on a combination of classical and modern control techniques, logic for mode switching, and diagnostics for failure detection to ensure safety and reliability, validated and verified through simulation and testing. A feedback control system is the quintessential cyberphysical system, where computing elements interact with the full complexity of the real world through noisy and limited communication channels.

Despite these successes, many applications of feedback control remain beyond the reach of modern tools and techniques. These applications may be highly under-sensed and under-actuated relative to the dimension of their significant dynamics; they may be difficult to model due to complex, unknown, or unpredictably changing physics; and they may require reliable high-performance control systems that must be engineered within tight deadlines and budgets. Adaptive control offers one potential solution to these challenges.

The underlying motivation for research in adaptive control is to develop control algorithms that respect sensor and actuator limitations, account for complex, uncertain, and unpredictably changing dynamics, and operate robustly despite noise. The promise of adaptive control is the ability to account for all of these effects and thereby reduce the time and cost needed to engineer reliable, high-performance feedback control systems for applications that are beyond the reach of fixed-gain feedback control laws.

While research on adaptive control spans the last 50 years with diverse techniques and demonstrated successes, the challenges are also well documented. Although no attempt is made here to survey the field, we cite [1] for a summary of challenges that researchers continue to address in order to make adaptive control a viable technology.

The goal of this paper is to provide a tutorial on retrospective cost adaptive control (RCAC). RCAC is a discrete-time adaptive control technique that is applicable to stabilization, command following, and disturbance rejection. As a discrete-time approach, RCAC is motivated by the desire to implement control algorithms that operate at the sensor sample rate without the need for controller discretization. This also means that the required modeling information can be estimated based on data sampled at the same rate as the control update. Adaptive control algorithms have been developed for discrete-time systems in [2]–[13]. In particular, the ability to handle plants with nonminimum-phase (NMP) zeros is demonstrated in [3]–[6], which is crucial for applications involving output feedback and for which positive real properties cannot be enforced.

II. HISTORICAL DEVELOPMENT OF RCAC

RCAC is based on the concept of *retrospectively optimized control*, where past controller coefficients used to generate past control inputs are *re-optimized* in the sense that *if* the re-optimized coefficients had been used over a previous window of operation, then the performance would have been better. Unlike signal processing applications such as estimation and identification, it is impossible to change past control inputs, and thus the re-optimized controller coefficients are used only to generate the next control input.

The idea of re-optimization is philosophically related to iterative feedback tuning (IFT) [14] and iterative learning control (ILC) [15]. However, unlike RCAC, IFT requires exogenous signals to estimate cost gradients, and ILC requires re-running the system under nearly identical initial conditions and exogenous inputs. Some elements of RCAC appear in [6].

RCAC was originally developed within the context of active noise control experiments [16]. The algorithm used in [16] is gradient-based, where the gradient direction and step size are based on different cost functions. In subsequent work [17], the gradient algorithm was replaced by batch least-squares optimization. In both [16] and [17], the modeling information is given by Markov parameters (impulse response coefficients) of the open-loop transfer function G_{zu} from the control input u to the performance variable z.

More recently, in [18], a recursive least squares algorithm was used, along with knowledge of the NMP zeros of G_{zu}. The approaches in [16], [17], [18] are closely related in the sense that all of the NMP zeros outside of the spectral radius of G_{zu} are approximate zeros of a polynomial whose coefficients are Markov parameters of G_{zu}.

RCAC uses a filter $G_{\rm f}$ to define the retrospective cost by filtering the difference between the actual past control inputs and the re-optimized control inputs. To construct $G_{\rm f}$, Markov parameters are used in [16], [17], and NMP zeros are used in [18]. As shown in [18], $G_{\rm f}$ serves as a *target model* for a closed-loop transfer function (called Γ) whose zeros include the zeros of G_{zu}. The need for $G_{\rm f}$ to include the NMP zeros arises from the fact that if a NMP zero of G_{zu} is *not* included

in $G_{\rm f}$, then RCAC tends to cancel the zero through feedback in order to match Γ.

The theoretical development of RCAC includes gradient optimization with Markov parameters [16], batch optimization with Markov parameters for NMP plants [17], and RLS optimization using the NMP zeros in $G_{\rm f}$ [18]. RCAC was applied to the Rohrs counterexamples in [19] and demonstrated for broadband disturbance rejection in [20]. Application of RCAC to Hammerstein plants with monotonic input nonlinearities is considered in [21]. Extensions to MIMO systems was considered in [22], where it is shown that RCAC squares nonsquare plants, which may introduce NMP squaring zeros.

RCAC has been implemented in both simulation and laboratory experiments. Numerical simulation studies are given in [23], [24] for flow control; in [25] for noncolocated control of a linkage; in [20], [26]–[28] for vibration control; in [29] for engine control; in [30]–[33] for aircraft control; in [34] for spacecraft control; in [35] for quadrotor control; in [36] for missile control; in [37] for scramjet control; and in [38] for control of systems with hysteresis. Laboratory experiments are reported in [16], [39], [40] for noise control; in [41] for ducted flame control; and in [42] for 6DOF motion control.

III. RCAC ALGORITHM

A. Standard Problem

Consider the standard problem consisting of the discrete-time, linear time-invariant system

$$x(k+1) = Ax(k) + Bu(k) + D_1w(k), \tag{1}$$
$$y(k) = Cx(k) + D_0u(k) + D_2w(k), \tag{2}$$
$$z(k) = E_1x(k) + E_2u(k) + E_0w(k), \tag{3}$$

where $x(k) \in \mathbb{R}^n$ is the state, $y(k) \in \mathbb{R}^{l_y}$ is the measurement, $u(k) \in \mathbb{R}^{l_u}$ is the control input, $w(k) \in \mathbb{R}^{l_w}$ is the exogenous input, and $z(k) \in \mathbb{R}^{l_z}$ is the measured performance variable. We say that w is matched with u if $D_1 = B$, $D_2 = D_0$, and $E_0 = E_2$. The goal is to develop an adaptive output feedback controller that minimizes z in the presence of the exogenous signal w with limited modeling information about (1)–(3). The components of w can represent either command signals to be followed, external disturbances to be rejected, or both, depending on the choice of D_1 and E_0. Depending on the application, components of w may or may not be measured. The measured components of w may be included in y by suitable choice of C and D_2. Since RCAC is an input-output approach to adaptive control, the controllability and observability of (1)–(3) does not play an explicit role. Figure 1 shows a block diagram of the standard problem with the adaptive controller $G_{{\rm c},k}$.
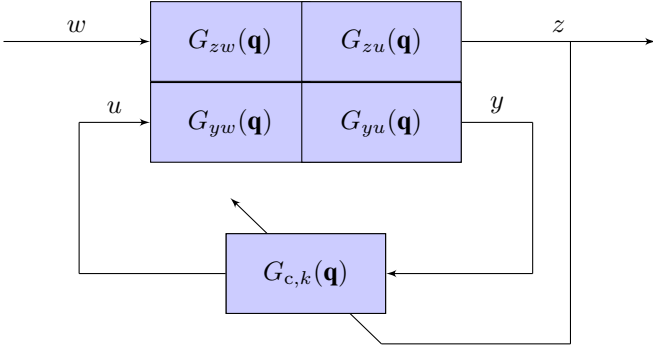
Fig. 1.   Transfer function representation of the adaptive standard problem with controller $G_{\mathrm{c},k}$.

B. Controller Structure

Define the dynamic compensator

$$u(k) = \sum_{i=1}^{n_{\mathrm{c}}} P_i(k)u(k-i) + \sum_{i=k_{\mathrm{c}}}^{n_{\mathrm{c}}} Q_i(k)y(k-i), \quad (4)$$

where $P_i(k) \in \mathbb{R}^{l_u \times l_u}$ and $Q_i(k) \in \mathbb{R}^{l_u \times l_y}$ are the controller coefficient matrices, and $k_{\mathrm{c}} \geq 0$. For controller startup, we implement (4) as

$$u(k) = \begin{cases} 0, & k < k_{\mathrm{w}}, \\ \Phi(k)\theta(k), & k \geq k_{\mathrm{w}}, \end{cases} \quad (5)$$

where the regressor matrix $\Phi(k)$ is defined by

$$\Phi(k) \triangleq \begin{bmatrix} u(k-1) \\ \vdots \\ u(k-n_{\mathrm{c}}) \\ y(k-k_{\mathrm{c}}) \\ \vdots \\ y(k-n_{\mathrm{c}}) \end{bmatrix}^{\mathrm{T}} \otimes I_{l_u} \in \mathbb{R}^{l_u \times l_\theta}, \quad (6)$$

k_{w} is an initial waiting period that allows $\Phi(k)$ to be populated with data, and the controller coefficient vector $\theta(k)$ is defined by

$$\theta(k) \triangleq \mathrm{vec}\left[P_1(k) \cdots P_{n_{\mathrm{c}}}(k) \; Q_{k_{\mathrm{c}}}(k) \cdots Q_{n_{\mathrm{c}}}(k) \right]^{\mathrm{T}} \in \mathbb{R}^{l_\theta}, \quad (7)$$

$l_\theta \triangleq l_u^2 n_{\mathrm{c}} + l_u l_y (n_{\mathrm{c}} + 1 - k_{\mathrm{c}})$, "$\otimes$" is the Kronecker product, and "vec" is the column-stacking operator. Note that $k_{\mathrm{c}} = 0$ allows an exactly proper controller, whereas $k_{\mathrm{c}} \geq 1$ yields a strictly proper controller of relative degree at least k_{c}. In all examples in this paper, we use $k_{\mathrm{c}} = 1$, and unless specified otherwise, we use $k_{\mathrm{w}} = n_{\mathrm{c}}$. In terms of the forward shift operator $\mathbf{q}$, the transfer function of the controller from y to u is given by

$$G_{\mathrm{c},k}(\mathbf{q}) = \left(\mathbf{q}^{n_{\mathrm{c}}} I_{l_u} - \mathbf{q}^{n_{\mathrm{c}}-1} P_1(k) - \cdots - P_{n_{\mathrm{c}}}(k) \right)^{-1} \\ \cdot \left(\mathbf{q}^{n_{\mathrm{c}}-k_{\mathrm{c}}} Q_{k_{\mathrm{c}}}(k) + \cdots + Q_{n_{\mathrm{c}}}(k) \right). \quad (8)$$

If y and u are scalar signals, then G_{c} is SISO and (8) can be written as

$$G_{\mathrm{c},k}(\mathbf{q}) = \frac{\mathbf{q}^{n_{\mathrm{c}}-k_{\mathrm{c}}} Q_{k_{\mathrm{c}}}(k) + \cdots + Q_{n_{\mathrm{c}}}(k)}{\mathbf{q}^{n_{\mathrm{c}}} - \mathbf{q}^{n_{\mathrm{c}}-1} P_1(k) - \cdots - P_{n_{\mathrm{c}}}(k)}. \quad (9)$$

C. Retrospective Performance Variable

We define the retrospective control as

$$\hat{u}(k, \hat{\theta}) = \Phi(k)\hat{\theta}, \quad (10)$$

where $\hat{\theta} \in \mathbb{R}^{l_\theta}$. The corresponding retrospective performance variable is defined as

$$\hat{z}(k, \hat{\theta}) \triangleq z(k) + G_{\mathrm{f}}(\mathbf{q})[\hat{u}(k, \hat{\theta}) - u(k)]. \quad (11)$$

The $n_z \times n_u$ filter G_{f} has the form

$$G_{\mathrm{f}} \triangleq D_{\mathrm{f}}^{-1} N_{\mathrm{f}}, \quad (12)$$

where D_{f} is an $l_z \times l_z$ polynomial matrix with leading coefficient I_{l_u}, and N_{f} is an $l_z \times l_u$ polynomial matrix. For reasons given below, we henceforth refer to G_{f} as the *target model*. By defining the filtered versions $\Phi_{\mathrm{f}}(k) \in \mathbb{R}^{l_z \times l_\theta}$ and $u_{\mathrm{f}}(k) \in \mathbb{R}^{l_z}$ of $\Phi(k)$ and $u(k)$, respectively, (11) can be written as

$$\hat{z}(k, \hat{\theta}) = z(k) + \Phi_{\mathrm{f}}(k)\hat{\theta} - u_{\mathrm{f}}(k), \quad (13)$$

where

$$\Phi_{\mathrm{f}}(k) \triangleq G_{\mathrm{f}}(\mathbf{q})\Phi(k), \quad u_{\mathrm{f}}(k) \triangleq G_{\mathrm{f}}(\mathbf{q})u(k). \quad (14)$$

The optimal controller coefficient vector $\hat{\theta}_{\mathrm{opt}}(k)$ is obtained by retrospective optimization below to yield the updated controller with coefficients

$$\theta(k+1) = \hat{\theta}_{\mathrm{opt}}(k). \quad (15)$$

D. Role of the Target Model G_{f}

The target model G_{f} is a key component of RCAC. In early work, G_{f} was viewed as a model of G_{zu} that captures the sign of the leading coefficient of G_{zu} along with the NMP zeros of G_{zu}. In [18], the analysis of RCAC involves an ideal filter G_{f}^*, which is a closed-loop transfer function involving an ideal feedback controller G_{c}^*. This insight leads to an alternative interpretation of G_{f}, where G_{f} is a target model for a specific closed-loop transfer function. These properties are summarized below for the case where z and u are scalar signals.

1) Frequency response: For a given choice of G_{f}, RCAC updates θ so that the frequency response of the transfer function Γ tends to match that of G_{f}, where

$$\Gamma(\mathbf{q}) \triangleq \frac{N_{zu}(\mathbf{q})\mathbf{q}^{n_{\mathrm{c}}}}{D_{\mathrm{c}}(\mathbf{q})D_{zu}(\mathbf{q}) + N_{\mathrm{c}}(\mathbf{q})N_{zu}(\mathbf{q})}, \quad (16)$$

and $G_{zu} = N_{zu}/D_{zu}$. The transfer function Γ is closely related to the closed-loop transfer function from an external perturbation v of u to the performance variable z. This transfer function is given by

$$G_{zv}(\mathbf{q}) = \frac{N_{zu}(\mathbf{q})D_{\mathrm{c}}(\mathbf{q})}{D_{\mathrm{c}}(\mathbf{q})D_{zu}(\mathbf{q}) + N_{\mathrm{c}}(\mathbf{q})N_{zu}(\mathbf{q})}. \quad (17)$$

Note that Γ differs from G_{zv} due to the replacement of D_c in the numerator of (16) by $\mathbf{q}^{n_c}$.

2) Pole placement: If the order of G_f is equal to the order $n + n_c$ of the closed-loop system, then RCAC attempts to place the closed-loop poles at the locations of the poles of G_f. Hence, G_f can be used for pole placement.

3) Relative degree: In [18], the relative degree of the target model G_f is chosen to match the relative degree of G_{zu}. Since the relative degree of Γ is equal to the relative degree of G_{zu}, it follows that the relative degree of G_f must be chosen in accordance with G_{zu}.

4) NMP zeros: In [18], the target model G_f is chosen such that N_u contains the NMP zeros of G_{zu}. A key feature of Γ is the presence of N_{zu} in the numerator. This means that, since RCAC adapts G_c in order to match Γ to G_f, RCAC may cancel NMP zeros that are not included in G_f. This observation motivates the desire to capture all NMP zeros of N_{zu} in the numerator of G_f.

5) Markov parameters: In [16], [17], G_f is based on the Markov parameters of G_{zu}. In particular, for each complex number $\mathbf{z}$ whose absolute value is greater than the spectral radius of A, it follows that

$$G(\mathbf{z}) = E_1(\mathbf{z}I - A)^{-1}B = \sum_{i=0}^{\infty} \frac{H_i}{\mathbf{z}^i}, \qquad (18)$$

where, for all, $i \geq 1$, the ith Markov parameter of G_{zu} is given by

$$H_i \triangleq E_1 A^{i-1} B. \qquad (19)$$

As shown in [17], a sufficiently large number of Markov parameters used in the FIR truncation $G_f(\mathbf{z}) = \sum_{i=0}^{n_f} \frac{H_i}{\mathbf{z}^i}$ of (18) can capture the locations of the NMP zeros of G_{zu}. This choice of G_f also gives the correct relative degree.

6) FIR Target Model: In the case where G_{zu} is minimum phase, we define the FIR target model

$$G_f(\mathbf{q}) \triangleq \frac{H_{d_{zu}}}{\mathbf{q}^{d_{zu}}}. \qquad (20)$$

In the case where G_{zu} is NMP, we define the FIR target model

$$G_f(\mathbf{q}) \triangleq \frac{H_{d_{zu}} N_{zu,u}(\mathbf{q})}{\mathbf{q}^{d_{zu}+\deg(N_{zu,u})}}. \qquad (21)$$

7) IIR Target Model for Pole Placement: RCAC attempts to place the poles of Γ at the locations of the poles of G_f. Note that the poles of Γ are equal to the closed-loop poles, that is, the poles of $\widetilde{G}_{zw}$. Consequently, RCAC attempts to place the closed-loop poles at the locations of the poles of G_f. In order to use G_f for pole placement, let D_p be a monic polynomial whose roots are the desired closed-loop pole locations. Then, in the case where G_{zu} is minimum phase, we define the IIR target model

$$G_f(\mathbf{q}) \triangleq \frac{H_{d_{zu}}}{\mathbf{q}^{d_{zu}-\deg(D_p)}D_p(\mathbf{q})}, \qquad (22)$$

and, in the case where G_{zu} is NMP, we define the IIR target model

$$G_f(\mathbf{q}) \triangleq \frac{H_{d_{zu}} N_{zu,u}(\mathbf{q})}{\mathbf{q}^{d_{zu}+\deg(N_{zu,u})-\deg(D_p)}D_p(\mathbf{q})}. \qquad (23)$$

The target models (20), (22) for minimum-phase G_{zu}, and (21), (23) for NMP G_{zu} represent the modeling information required by RCAC.

E. Retrospective Cost

Using the retrospective performance variable $\hat{z}(k,\hat{\theta})$ defined by (11), we define the cumulative retrospective cost function

$$J(k,\hat{\theta}) \triangleq \sum_{i=1}^{k} \lambda^{k-i}[\hat{z}^T(i,\hat{\theta})R_z\hat{z}(i,\hat{\theta}) + (\Phi_f(i)\hat{\theta})^T R_u \Phi_f(i)\hat{\theta}]$$
$$+ \lambda^k(\hat{\theta} - \theta(0))^T R_\theta(\hat{\theta} - \theta(0)), \qquad (24)$$

where R_z and R_θ are positive definite, R_f is a positive semidefinite performance dependent weight, and $\lambda \in (0, 1]$ is the forgetting factor. Recursive minimization of (24) is used to update the controller coefficients $\theta(k)$.

Proposition: Let $P(0) = R_\theta^{-1}$. Then, for all $k \geq 1$, the retrospective cost function (24) has a unique global minimizer $\theta(k)$, which is given by

$$\theta(k) = \theta(k-1) - P(k-1)\Phi_f^T(k)\Upsilon^{-1}(k)[\Phi_f(k)\theta(k-1)$$
$$+ (R_z + R_u)^{-1}R_z(z(k) - u_f(k))], \quad (25)$$

$$P(k) = \frac{1}{\lambda}P(k-1) -$$
$$\frac{1}{\lambda}P(k-1)\Phi_f^T(k)\Upsilon^{-1}(k)\Phi_f(k)P(k-1), \quad (26)$$

where

$$\Upsilon(k) \triangleq \lambda(R_z + R_u)^{-1} + \Phi_f(k)P(k-1)\Phi_f^T(k).$$

Notice that, if $\lambda = 1$, then the covariance $P(k)$ decreases monotonically, which decreases the rate of adaptation as θ converges. To maintain adaptation in cases where the plant or exogenous signals are changing, the covariance can be reset using suitable logic. Alternatively, setting the forgetting factor $\lambda < 1$ prevents monotonic decrease of $P(k)$, but can lead to instability, especially in the presence of noise and in the absence of persistency. An alternative approach is to include an additional positive-semidefinite forcing term Q on the right-hand side of (26) of the form

$$P(k) = P(k-1) -$$
$$P(k-1)\Phi_f^T(k)\Upsilon^{-1}(k)\Phi_f(k)P(k-1) + Q, \quad (27)$$

where $\lambda = 1$ in $\Upsilon(k)$. Note that (25) and (27) is the Kalman filter Riccati update equations with the dynamics matrix $A = I_{l_\theta}$ and output matrix $C(k) = \Phi_f(k)$. Consequently, persistency in (25) is determined by the observability of (I_{l_θ}, Φ_f). For all examples in this paper, we initialize $\theta(0) = 0$, and, unless specified otherwise, we choose $R_u = 0$.

IV. Command-Following

A. The Adaptive Servo Problem

Consider the discrete-time, linear time-invariant system

$$x(k+1) = Ax(k) + Bu(k) + \bar{D}_1 d(k), \tag{28}$$

$$y_0(k) = \bar{C}x(k) + \bar{D}_0 u(k) + \bar{D}_2 d(k), \tag{29}$$

$$y_{\mathrm{n}}(k) = y_0(k) + v(k), \tag{30}$$

$$z(k) = r(k) - y_0(k), \tag{31}$$

where $x(k) \in \mathbb{R}^n$ is the state, $y_{\mathrm{n}}(k) \in \mathbb{R}^{l_y}$ is the measurement, $u(k) \in \mathbb{R}^{l_u}$ is the control input, $d(k) \in \mathbb{R}^{l_d}$ is the disturbance, $r(k) \in \mathbb{R}^{l_y}$ is the command, $v(k) \in \mathbb{R}^{l_y}$ is the sensor noise, and $z(k) \in \mathbb{R}^{l_y}$ is the performance variable. We can rewrite (30) in terms of $\mathbf{q}$ as

$$y_0(k) = G_u(\mathbf{q})u(k) + G_d(\mathbf{q})d(k), \tag{32}$$

where

$$G_u(\mathbf{q}) \triangleq \bar{C}(\mathbf{q}I - A)^{-1}B + \bar{D}_0, \tag{33}$$

$$G_d(\mathbf{q}) \triangleq \bar{C}(\mathbf{q}I - A)^{-1}\bar{D}_1 + \bar{D}_2. \tag{34}$$

Furthermore, the linear time-invariant controller has the form

$$u(k) = G_{\mathrm{c}}(\mathbf{q})z(k), \tag{35}$$

where

$$z(k) \triangleq r(k) - y_{\mathrm{n}}(k). \tag{36}$$
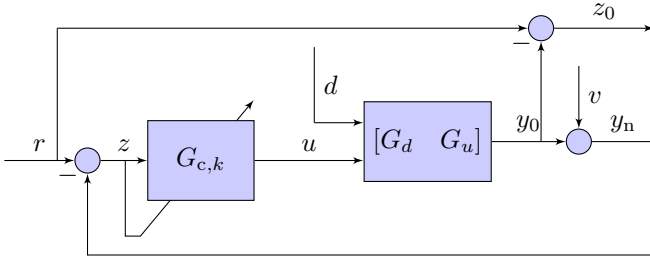
Figure 2 illustrates (32)–(36).

Fig. 2. Transfer function representation of the adaptive servo problem with the adaptive controller $G_{\mathrm{c},k}$.

The adaptive servo problem is thus a special case of the adaptive standard problem with

$$G_{zw} = [I_{l_y} \quad -G_d \quad 0], \quad G_{zu} = -G_u, \tag{37}$$

$$G_{yw} = [I_{l_y} \quad -G_d \quad -I_{l_y}], \quad G_{yu} = -G_u. \tag{38}$$

B. Command Following for Minimum-Phase Plants

Example 1. *Effect of R_θ on command-following performance for a step command.* Consider the asymptotically stable, minimum-phase plant

$$G(\mathbf{q}) = \frac{\mathbf{q} - 0.85}{(\mathbf{q} - 0.8)(\mathbf{q} - 0.9)}. \tag{39}$$

Let r be a unit-height step command, and let $d = v = 0$. We use the FIR target model (20), and set $n_{\mathrm{c}} = 3$. Figure

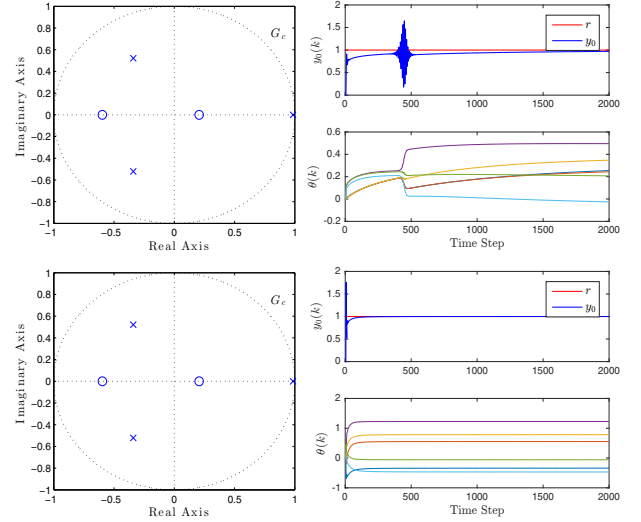3 shows the command-following performance for $R_\theta = 20$ and $R_\theta = 0.2$. ∎

Fig. 3. Example 1: Effect of R_θ on command-following performance for a step command for (39). For $R_\theta = 20$ (upper plots), RCAC follows the step command in about 2000 time steps, whereas, for $R_\theta = 0.2$ (lower plots), RCAC follows the step command in about 200 time steps. For both values of R_θ, the converged controllers have integrators, as shown by the poles at 1.

Example 2. *Effect of R_u on command-following performance for a harmonic command.* Consider the asymptotically stable, minimum-phase plant

$$G(\mathbf{q}) = \frac{\mathbf{q} - 0.8}{(\mathbf{q} - 0.95)(\mathbf{q} - 0.99)}. \tag{40}$$

Let r be the harmonic command $r(k) = \cos \omega k$, where $\omega = 0.5$ rad/sample, and let $d = v = 0$. We use the FIR target model (20), and set $n_{\mathrm{c}} = 5$ and $R_\theta = 0.2$. Figure 4 shows the command-following performance for $R_u = 0$ and $R_u = 0.1$. ∎

Example 3. *Minimum-phase zero cancellation.* Consider the unstable, minimum-phase plant

$$G(\mathbf{q}) = \frac{(\mathbf{q} - 0.6)(\mathbf{q} - 0.8)}{(\mathbf{q} - 1.1)(\mathbf{q}^2 - 1.6\mathbf{q} + 1)}. \tag{41}$$

Let r be the harmonic command $r(k) = \cos \omega k$, where $\omega = 0.6$ rad/sample, and let $d = v = 0$. We use the FIR target model (20), and set $n_{\mathrm{c}} = 16$ and $R_\theta = 2 \times 10^{-7}$. Figure 5 shows the command-following performance. Since the minimum-phase zeros of G_{zu} are not included in the numerator of G_{f}, RCAC adapts G_{c} so that they are cancelled. ∎

Example 4. *Including an internal model.* Example 1 shows that RCAC can develop an internal model of the command. However, to speed up convergence, we can include
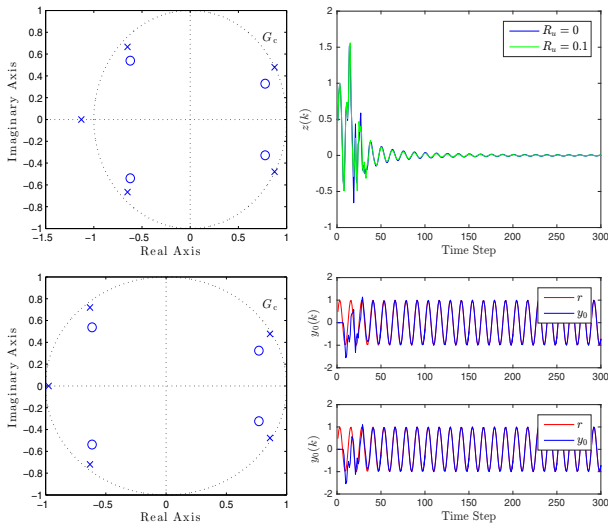
Fig. 4. Example 2: Effect of R_u on command-following performance for a harmonic command for (40). For $R_u = 0$ (upper plots), RCAC converges to an unstable controller, with an unstable pole at -1.13 and an internal model of the harmonic command, whereas, for $R_u = 0.1$ (lower plots), RCAC converges to an asymptotically stable controller without an internal model and thus with a nonzero command-following error. The lower left plot shows the command-following response for both $R_u = 0$ (upper) as well as $R_u = 0.1$ (lower).
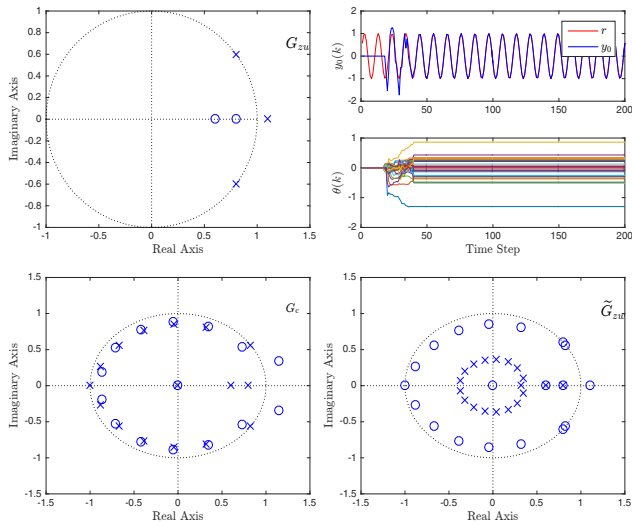
Fig. 5. Example 3: Minimum-phase zero cancellation. Since the minimum-phase zeros of G_{zu} are not included in the numerator of G_f, RCAC places closed-loop poles at the location of the minimum-phase zeros of G_{zu}.

an internal model in the controller. For example, to embed integrators in the controller, we introduce the integrator states

$$\gamma(k) = \gamma(k-1) + Fy(k), \qquad (42)$$

where $\gamma(k) \in \mathbb{R}^{l_\gamma}$ and $F \in \mathbb{R}^{l_\gamma \times l_y}$ selects components of $y(k)$. We then cascade (42) with (4) by means of a gain $K_\mathrm{I}(k) \in \mathbb{R}^{l_\gamma}$ to obtain

$$u(k) = \sum_{i=1}^{n_c} P_i(k)u(k-i) + \sum_{i=k_0}^{n_c} Q_i(k)y(k-i) + K_\mathrm{I}(k)\gamma(k). \qquad (43)$$

We then augment $\Phi(k)$ and $\theta(k)$ accordingly. Consider the asymptotically stable, minimum-phase plant

$$G(\mathbf{q}) = \frac{(\mathbf{q}-0.8)(\mathbf{q}-0.9)}{(\mathbf{q}-0.4)(\mathbf{q}^2+0.16)}. \qquad (44)$$

Let r be a unit-height step command, and let $d = v = 0$. We use the FIR target model (20), and set $n_c = 4$ and $R_\theta = 10$. Figure 6 shows the command-following performance, in the case where RCAC converges to a controller with an integrator, as well in the case where an integrator is included in the controller. ∎
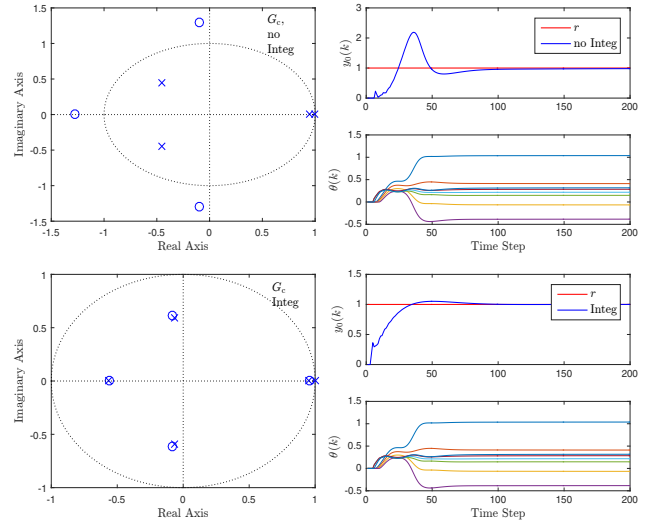

Fig. 6. Example 4: Including an internal model. In both cases, RCAC follows the step command. However, the command-following performance is improved in the case where an integrator is added.

C. NMP Plants

Example 5. *Command following for a plant with one real NMP zero.* Consider the asymptotically stable, NMP plant

$$G(\mathbf{q}) = \frac{(\mathbf{q}-1.05)(\mathbf{q}-0.8)}{(\mathbf{q}-0.85)(\mathbf{q}-0.88)(\mathbf{q}-0.9)}. \qquad (45)$$

Let r be a unit-height step command, and let $d = v = 0$. We use the FIR target model (21), and set $n_c = 5$ and $R_\theta = 200$. Figure 7 shows the command-following performance. ∎
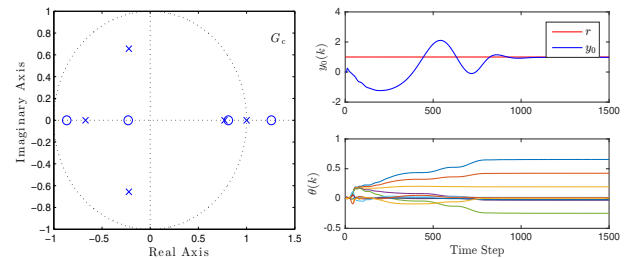

Fig. 7. Example 5: Command following for a plant with one real NMP zero. G_f is constructed to have the same NMP zero as (45). RCAC develops an internal model and follows the step command.

Example 6. *Command following for a plant with one NMP zero, using Markov parameters for the target model.* Consider the asymptotically stable, NMP plant

$$G(\mathbf{q}) = \frac{(\mathbf{q} - 1.1)(\mathbf{q} - 0.6)}{(\mathbf{q} - 0.7)(\mathbf{q} - 0.8)(\mathbf{q} - 0.9)}. \qquad (46)$$

Let r be a unit-height step command, and let $d = v = 0$. We use 60 Markov parameters for the target model, which allows G_f to capture the location of the NMP zero at 1.1. We set $R_\theta = 140$ and $n_c = 20$. Figure 47 shows the command-following performance. ∎
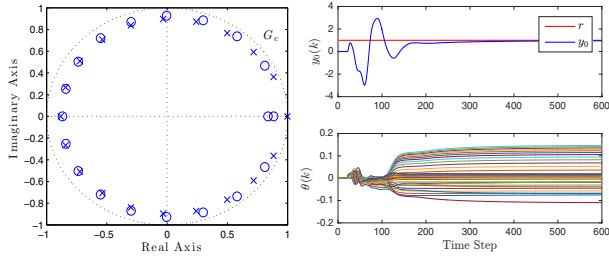
Fig. 8. Example 6: Command following for a plant with one NMP zero, using Markov parameters for the target model, for (46). RCAC follows the step command.

Example 7. *Command following for a plant with two complex NMP zeros.* Consider the asymptotically stable, NMP plant

$$G(\mathbf{q}) = \frac{(\mathbf{q} - 1 + 1.1\jmath)(\mathbf{q} - 1 - 1.1\jmath)}{(\mathbf{q} - 0.7)(\mathbf{q} - 0.85)(\mathbf{q} - 0.95)}. \qquad (47)$$

Let r be the harmonic command $r(k) = \cos \omega k$, where $\omega = 0.2$ rad/sample, and let $d = v = 0$. We use the FIR target model (21), and set $R_\theta = 10$ and $n_c = 12$. Figure 9 shows the command-following performance. ∎
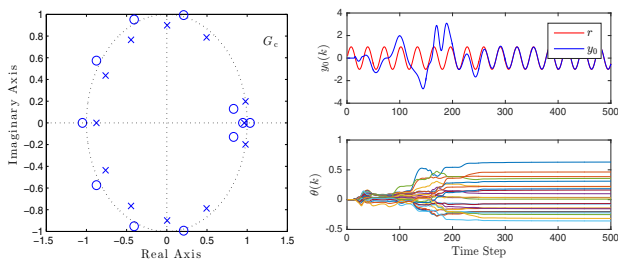

Fig. 9. Example 7: Command following for a plant with two complex NMP zeros. (47) has two complex NMP zeros, which are used in the target model. RCAC follows the harmonic command.

Example 8. *Command following for an unstable NMP plant that requires an unstable controller.* Consider the unstable, NMP plant

$$G(\mathbf{q}) = \frac{(\mathbf{q} - 0.6)(\mathbf{q} - 0.8)(\mathbf{q} - 1.05)}{(\mathbf{q} - 0.9)(\mathbf{q} - 1.1)(\mathbf{q}^2 - 1.6\mathbf{q} + 0.89)}. \qquad (48)$$

Note that the NMP zero lies between 1 and the unstable pole. It follows from root locus analysis and the parity

interlacing property [44] that, in order to stabilize this plant, the controller must be unstable [4]. Let r be the harmonic command $r(k) = \cos \omega k$, where $\omega = 0.6$ rad/sample, and let $d = v = 0$. We use the FIR target model (21), and set $R_\theta = 2 \times 10^{-7}$ and $n_c = 16$. Figure 10 shows the command-following performance. ∎
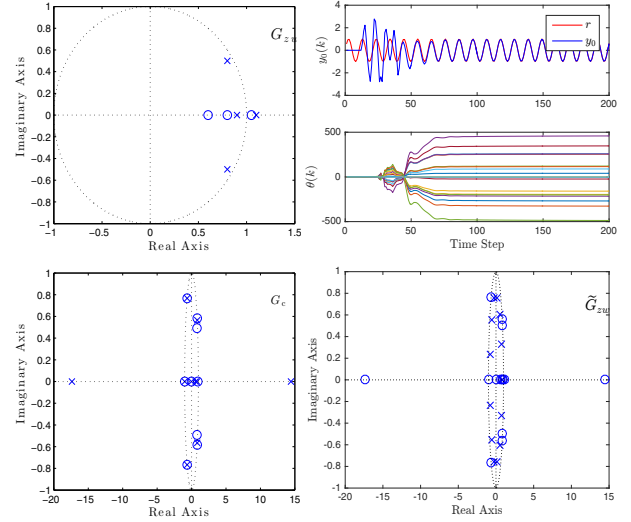

Fig. 10. Example 8: Command following for an unstable NMP plant whose stabilization requires an unstable controller. Notice that RCAC places an unstable controller pole to the right of the unstable plant pole, and that the closed-loop system is asymptotically stable.

D. Adaptive Feedforward Control

In this section we consider extensions of the adaptive servo problem to include feedforward control. The first feedforward architecture uses centralized adaptation, as shown in Figure 11.
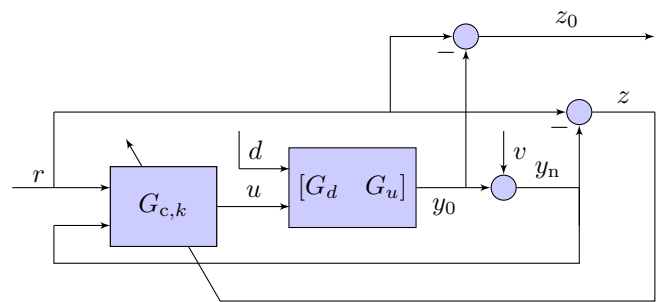

Fig. 11. Transfer function representation of centralized feedback-feedforward control for the adaptive servo problem.

Alternatively, RCAC may use a decentralized feedback and feedforward architecture that allows for decentralized adaptation, as shown in Figure 12. In this case, the feedback controller $G_{\mathrm{fb},k}$ may have poles that are different from those of the feedforward controller $G_{\mathrm{ff},k}$, which is not possible with centralized feedback-feedforward control. Moreover, we may choose the feedback controller to be FIR.
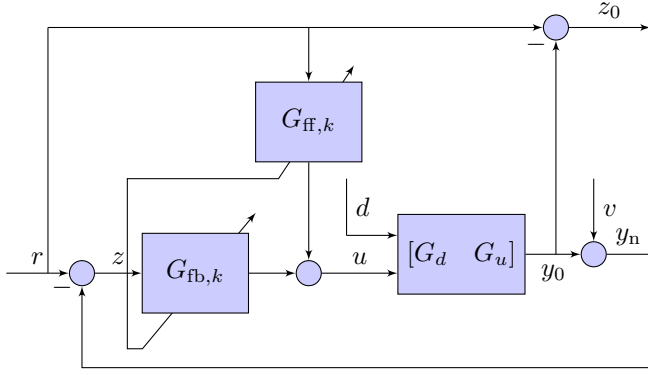
Fig. 12. Transfer function representation of decentralized feedback-feedforward control for the adaptive servo problem.

The model reference adaptive control (MRAC) problem is a special case of the adaptive standard problem with

$$w = \begin{bmatrix} r \\ d \\ v \end{bmatrix}, \quad y = \begin{bmatrix} r \\ y_n \end{bmatrix}, \quad z = G_m r - y_n, \quad (49)$$

$$G_{zw} = [G_m \quad -G_d \quad -I_{l_z}], \quad G_{zu} = -G_u, \quad (50)$$

$$G_{yw} = \begin{bmatrix} I_{l_r} & 0 & 0 \\ 0 & G_d & I_{l_z} \end{bmatrix}, \quad G_{yu} = G_u, \quad (51)$$

where $r \in \mathbb{R}^{l_r}$ and G_m is the reference model. Figure 13 shows the transfer function representation of the MRAC problem. Note that, since y includes the command r, the controller is both feedback and feedforward.
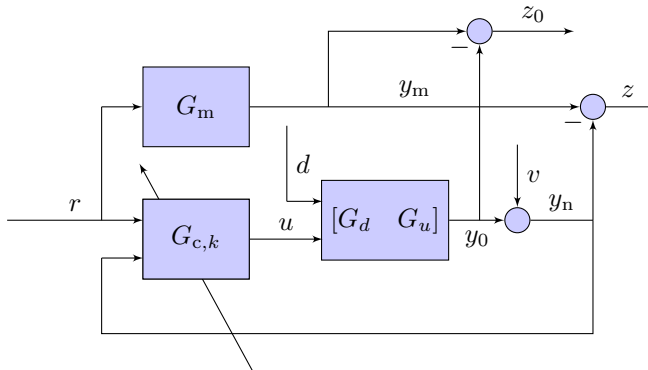

Fig. 13. Transfer function representation of the model reference adaptive control problem with the adaptive controller $G_{c,k}$.

Example 9. *Command following using centralized feedback-feedforward control for the adaptive servo problem.* Consider the asymptotically stable, NMP plant

$$G(\mathbf{q}) = \frac{(\mathbf{q} - 1.2)(\mathbf{q}^2 - 1.8\mathbf{q} + 0.85)}{(\mathbf{q} - 0.9)(\mathbf{q} - 0.95)(\mathbf{q}^2 - 1.4\mathbf{q} + 0.74)}. \quad (52)$$

Let r be the harmonic command $r(k) = \cos \omega k$, where $\omega = 0.4$ rad/sample, and let $d = v = 0$. We apply the centralized feedback-feedforward control architecture shown in Figure 11 with $R_\theta = 10$ and $n_c = 8$, and we use the FIR

target model (21). Figure 14 shows the command-following performance for combined feedforward and feedback control. RCAC follows the harmonic command without developing an internal model. ∎
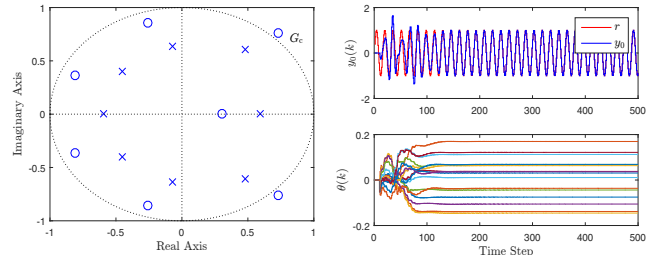

Fig. 14. Example 9: Combined feedforward and feedback control. RCAC follows the harmonic command without developing an internal model.

Example 10. *Command following using decentralized feedback-feedforward control for the adaptive servo problem.* Consider the asymptotically stable, NMP plant

$$G(\mathbf{q}) = \frac{(\mathbf{q} - 0.9)(\mathbf{q} - 1.1)}{(\mathbf{q} - 0.99)(\mathbf{q}^2 - 1.9\mathbf{z} + 0.9925)}. \quad (53)$$

Let r be a unit-height step command, and let $d = v = 0$. We apply the decentralized feedback-feedforward control architecture shown in Figure 12. For both controllers we set $R_\theta = 10^5$ and $n_c = 10$, and we use the FIR target model (20). We restrict G_{fb} to be an FIR controller. Figure 15 shows the command-following performance. Note that, since the feedback controller is FIR, RCAC cannot develop an internal model of the command. However, RCAC adapts G_{ff} so that the command is followed. ∎
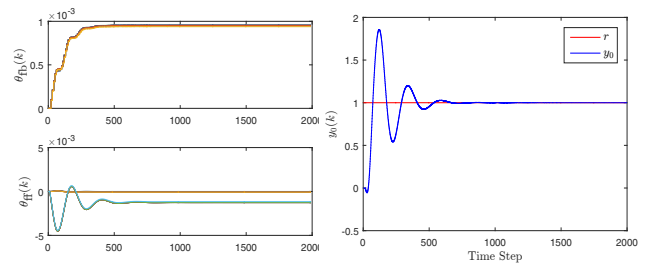

Fig. 15. Example 10: Command following using decentralized feedback-feedforward control for the adaptive servo problem. Since the feedback controller is FIR, RCAC cannot develop an internal model of the command. However, RCAC adapts G_{ff} so that the command is followed.

Example 11. *MRAC with step disturbance.* Consider the unstable, minimum-phase double integrator

$$G(\mathbf{q}) = \frac{\mathbf{q} - 0.95}{(\mathbf{q} - 1)^2}. \quad (54)$$

Let r be a sequence of step commands with different heights, let $d = 0.2$, and let $v = 0$. Let G_m be the continuous-time reference model $M(s) = \frac{1}{s^2 + 2s + 1}$ discretized with sampling period $h = 0.5$ sec. We set $R_\theta = 0.1$ and $n_c = 12$, and we use the FIR target model (20). RCAC rejects the step

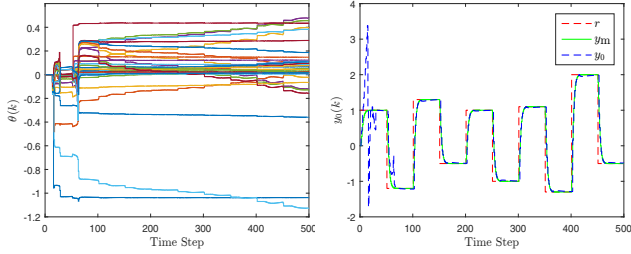disturbance and follows the output of the reference model, as shown in Figure 16. ∎

Fig. 16. Example 11: MRAC with step disturbance. RCAC rejects the step disturbance, and follows the output of the reference model.

Example 12. *MRAC for a NMP plant.* Consider the unstable, NMP double integrator

$$G(\mathbf{q}) = \frac{\mathbf{q} - 1.1}{(\mathbf{q} - 1)^2}. \tag{55}$$

Let r be a sequence of step commands with different heights, and let $d = v = 0$. Let G_{m} be the continuous-time reference model $M(s) = \frac{1}{s^2 + 30s + 1}$ discretized with sampling period $h = 1$ sec. We set $R_\theta = 10^{-3}$ and $n_{\mathrm{c}} = 8$, and we use the FIR target model (21). RCAC follows the output of the reference model, as shown in Figure 17. ∎

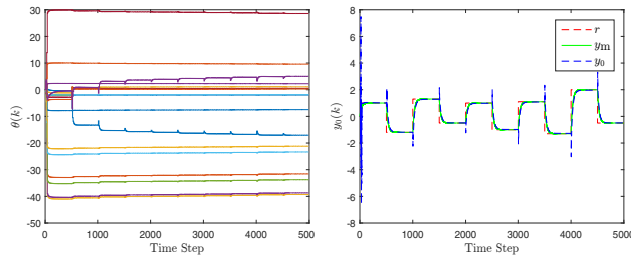Fig. 17. Example 12: MRAC for the unstable, NMP plant (55). RCAC follows the output of the reference model.

E. Pole Placement and Controller Poles

Example 13. *Pole placement for the adaptive servo problem.* Consider the unstable, minimum-phase plant

$$G(\mathbf{q}) = \frac{\mathbf{q}^2 - 1.4\mathbf{q} + 0.85}{(\mathbf{q} - 1.05)(\mathbf{q}^2 - 1.6\mathbf{q} + 0.89)}. \tag{56}$$

Let r be a unit step command, and let $d = v = 0$. To place five closed-loop poles at $0.05, 0.4, 0.6$, and $\pm 0.05\jmath$, we use the IIR target model (22) with

$$D_{\mathrm{p}}(\mathbf{q}) = (\mathbf{q} - 0.05)(\mathbf{q} - 0.4)(\mathbf{q} - 0.6)(\mathbf{q}^2 + 0.0025), \tag{57}$$

and set $R_\theta = 10^{-40}$ and $n_{\mathrm{c}} = 4$. RCAC follows the step command and places closed-loop poles near the locations of the roots of D_{p}, as shown in Figure 18. Note that two
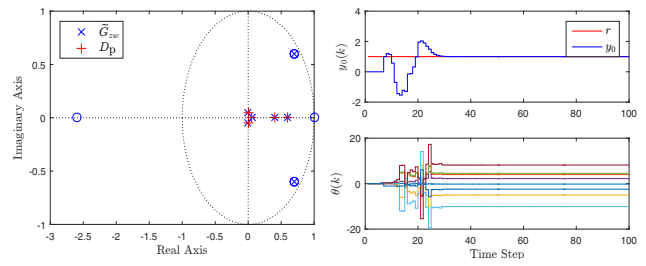

Fig. 18. Example 13: Pole placement for the adaptive servo problem. RCAC places five closed-loop poles near the locations of the roots of D_{p}. The closed-loop poles and zeros are shown at step $k = 100$.

closed-loop poles cancel the minimum-phase zeros of G. ∎

Example 14. *Choice of closed-loop poles leading to an unstable controller.* Consider the asymptotically stable, NMP plant given by (45), let r be a unit-height step command, and let $d = v = 0$. We use the FIR target model (21), and set $n_{\mathrm{c}} = 5$ and $R_\theta = 10$. Figure 19 shows the command-following performance. RCAC converges to an unstable controller, and the closed-loop poles do not converge to zero. ∎
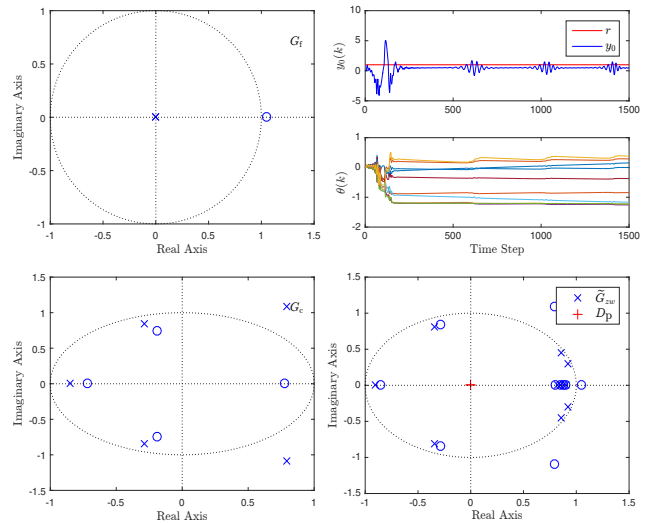

Fig. 19. Example 14: Choice of closed-loop poles leading to an unstable controller for (45). The choice of the target pole locations at zero causes RCAC to develop an unstable controller. RCAC does not follow the command, and the closed-loop poles do not converge to zero.

Example 15. *Choice of closed-loop poles leading to an asymptotically stable controller.* Consider the asymptotically stable, NMP plant given by (45), let r be a unit-height step command, and let $d = v = 0$. To place five closed-loop poles at 0.95, we use the IIR target model (23) with

$$D_{\mathrm{p}}(\mathbf{q}) = (\mathbf{q} - 0.95)^4, \tag{58}$$

and set $n_{\mathrm{c}} = 5$ and $R_\theta = 10$. Figure 20 shows the command-following performance. The choice of the target pole locations allows RCAC to develop an internal model

of the command, and $G_{c,k}$ converges to an asymptotically stable controller. RCAC places closed-loop poles near the locations of the poles of G_f. ∎
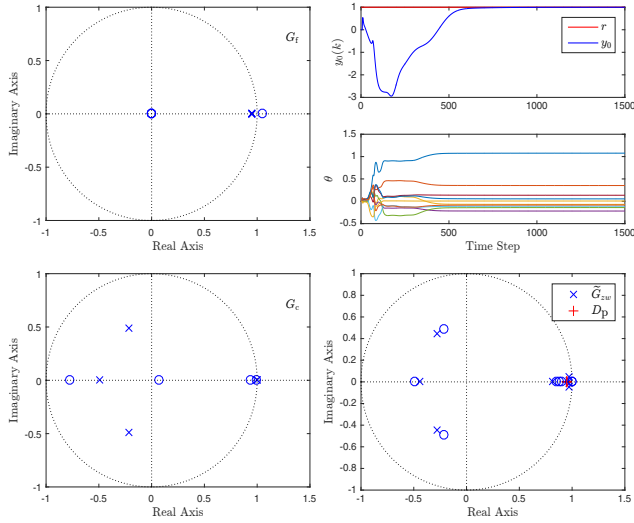

Fig. 20. Example 15: Choice of closed-loop poles leading to an asymptotically stable controller for (45). The choice of the target pole locations allows RCAC to develop an internal model of the command, and converge to a stable controller. RCAC places closed-loop poles near the locations of the poles of G_f.

Example 16. *Frequency response matching of G_f and Γ.* Consider the asymptotically stable, NMP plant

$$G(\mathbf{q}) = \frac{(\mathbf{q} - 0.99)(\mathbf{q} - 1.15)}{(\mathbf{q} - 0.88)(\mathbf{q} - 0.9)(\mathbf{q} - 0.95)}. \qquad (59)$$

Let r be the harmonic command $r(k) = \cos \omega k$, where $\omega = 0.6$ rad/sample, and let $d = v = 0$. We use the IIR target model (23) with

$$D_p(\mathbf{q}) = (\mathbf{q} - 0.5)(\mathbf{q} + 0.5)(\mathbf{q} + 0.5\jmath)(\mathbf{q} - 0.5\jmath), \qquad (60)$$

and set $n_c = 5$ and $R_\theta = 10^{-10}$. Figure 21 shows the command-following performance. The frequency response of Γ nearly matches the frequency response of G_f, particularly in magnitude. RCAC places closed-loop poles near the poles of G_f. ∎

F. Command Following for Nonlinear Plants

Example 17. *Command following for the Van der Pol oscillator, with a command whose phase portrait is inside the limit cycle.* Consider the discretized Van der Pol oscillator

$$x_1(k) = x_1(k-1) + T_s x_2(k-1), \qquad (61)$$
$$x_2(k) = x_2(k-1) + T_s((1 - x_1(k-1)^2)x_2(k-1)$$
$$- x_1(k-1) + u(k-1)), \qquad (62)$$

where $T_s = 0.01$ sec, $y_0(k) = x_2(k)$, $z(k) = r(k) - y_0(k)$, let r be a unit-amplitude harmonic command with frequency $\omega = 0.002$ rad/sample, and let $d = v = 0$. We use the FIR
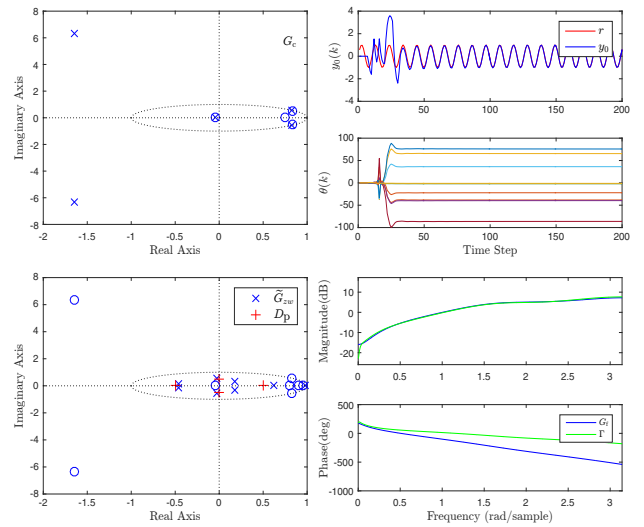

Fig. 21. Example 16: Frequency response matching of G_f and Γ for (59). The frequency response of Γ nearly matches the frequency response of G_f, particularly in magnitude. RCAC places closed-loop poles near the poles of G_f.

target model (20), and set $n_c = 10$ and $R_\theta = 1$. Figure 22 shows the command-following performance. ∎
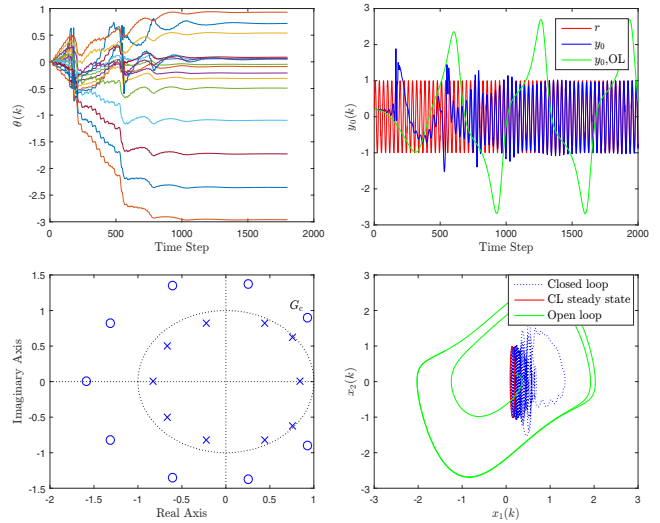

Fig. 22. Example 17: Command following for the Van der Pol oscillator (61)–(62), with a command whose phase portrait is inside the limit cycle. RCAC develops an internal model and follows the harmonic command. The lower plot shows the phase portraits of the open-loop limit cycle and the closed-loop response.

Example 18. *Command following for the Van der Pol oscillator, with a command whose phase portrait is outside the limit cycle.* Consider the discretized Van der Pol oscillator where $T_s = 0.005$ sec, $y_0(k) = x_2(k)$, $z(k) = r(k) - y_0(k)$, let r be a unit-amplitude harmonic command with frequency $\omega = 0.0008$ rad/sample, and let $d = v = 0$. We use the FIR target model (20), and set $n_c = 20$ and $R_\theta = 1$. Figure 23 shows the command-following performance. ∎
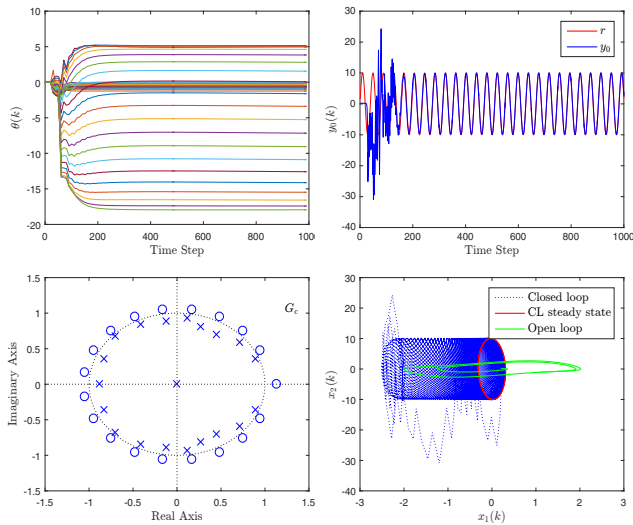
Fig. 23. Example 18: Command following for the Van der Pol oscillator (61)–(62), with a command whose phase portrait is outside the limit cycle. RCAC develops an internal model and follows the harmonic command. The lower plot shows the phase portraits of the open-loop limit cycle and the closed-loop response.
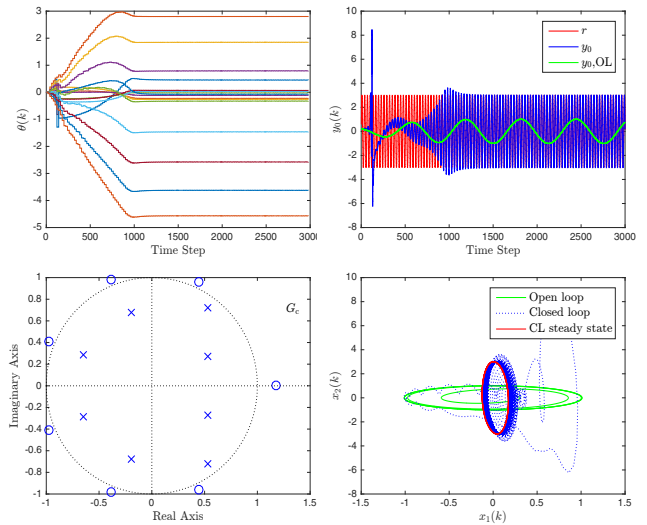

Fig. 24. Example 19: Command following for the Roup oscillator (63)–(64). The lower plot shows the phase portraits of the open-loop limit cycle and the closed-loop response. The open-loop plant approaches the harmonic limit cycle, and RCAC follows the harmonic command.

Example 19. *Command following for the Roup oscillator.* Consider the discretized oscillator from [43]

$$x_1(k) = x_1(k-1) + T_s x_2(k-1), \tag{63}$$

$$
\begin{aligned}
x_2(k) = x_2(k-1) + T_s[&-x_1(k-1) + u(k-1) \\
&- \lambda\big(x_1^2(k-1) + \omega^{-2}x_2^2(k-1) - a^2\big)x_2(k-1)],
\end{aligned} \tag{64}
$$

where $T_s = 0.01$ sec. Without control, this oscillator has a harmonic limit cycle with amplitude a and frequency ω. The parameter λ adjusts the rate of convergence to the limit cycle. Let $\lambda = 0.5$, $a = 1$, and $\omega = 1$. Let $y_0(k) = x_2(k)$, $z(k) = r(k) - y_0(k)$, let r be a unit-amplitude harmonic command with frequency $\omega = 0.002$ rad/sample, and let $d = v = 0$. We construct the target model using three Markov parameters, and set $n_c = 8$ and $R_\theta = 10$. Figure 24 shows the command-following performance for the initial condition $x(0) = [0.3 \quad 0.3]^T$. The open-loop plant approaches the harmonic limit cycle, and RCAC follows the harmonic command. ■

Example 20. *Command following for the Duffing oscillator.* Consider the discretized Duffing oscillator with constant disturbance

$$x_1(k) = x_1(k-1) + T_s x_2(k-1), \tag{65}$$

$$
\begin{aligned}
x_2(k) = x_2(k-1) + T_s[&-\frac{1}{4}x_2(k-1) + 4x_1(k-1) \\
&- x_1^3(k-1) + u(k-1) + 1],
\end{aligned} \tag{66}
$$

where $T_s = 0.01$ sec. The uncontrolled plant has stable equilibria at $(-1.86, 0)$ and $(2.11, 0)$. Let $y_0(k) = x_2(k)$, $z(k) = r(k) - y_0(k)$, let r be a unit-amplitude harmonic command with frequency $\omega = 0.0025$ rad/sample, and let

$v = 0$. We construct the target model using ten Markov parameters, and set $n_c = 10$ and $R_\theta = 100$. Figure 25 shows the command-following performance for the initial condition $x(0) = [0.1 \quad 0.1]^T$. The open-loop plant approaches the equilibrium at $(2.11, 0)$. RCAC follows the harmonic command. ■
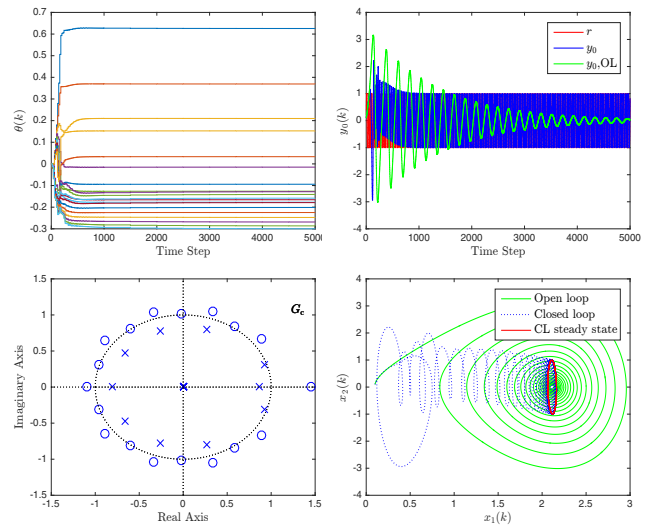

Fig. 25. Example 20: Command following for the Duffing oscillator (65)–(66). RCAC follows the harmonic command. The lower plot shows the phase portraits of the open-loop limit cycle and the closed-loop response. The open-loop plant approaches the equilibrium at $(2.11, 0)$.

V. DISTURBANCE REJECTION

A. Step Disturbance Rejection

In this section we consider step disturbance rejection, where the disturbance is a unit-height step. We consider the case where $y = z$ and with w matched with u.

Example 21. *Step disturbance rejection.* Consider the asymptotically stable, minimum-phase plant

$$G(\mathbf{q}) = \frac{\mathbf{q}^2 - 1.44\mathbf{q} + 0.81}{(\mathbf{q} - 0.9)(\mathbf{q}^2 - 1.71\mathbf{q} + 0.903)}, \quad (67)$$

To place four closed-loop poles at ± 0.5 and $\pm 0.8\jmath$, we use the IIR target model (22) with

$$D_\mathrm{p}(\mathbf{q}) = (\mathbf{q} - 0.5)(\mathbf{q} + 0.5)(\mathbf{q}^2 + 0.64), \quad (68)$$

and set $n_\mathrm{c} = 4$ and $R_\theta = 10^{-10}$. Figure 26 shows the closed-loop response. ∎
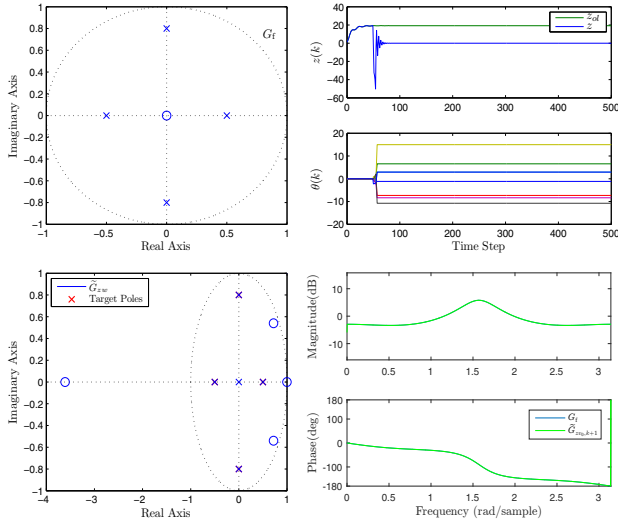

Fig. 26. Example 21: Step disturbance rejection for (67). The poles of G_f are achieved in $\widetilde{G}_{zw}$. The remaining unassigned assignable closed-loop poles converge to zero. The frequency response of Γ matches the frequency response of G_f.

Example 22. *Step disturbance rejection for an unstably stabilizable plant.* Consider the unstable, NMP plant

$$G(\mathbf{q}) = \frac{\mathbf{q} - 1.2}{(\mathbf{q} - 1.1)(\mathbf{q} - 2)}. \quad (69)$$

Let w be a unit step. We set $R_\theta = 10^{-40}$ and $n_\mathrm{c} = 3$. To place five closed-loop poles at $0.05, 0.4, 0.6,$ and $\pm 0.01\jmath$, we use the IIR target model (23) with four target closed-loop poles given by the roots of

$$D_\mathrm{p}(\mathbf{q}) = (\mathbf{q} - 0.4)(\mathbf{q} - 0.6)(\mathbf{q} - 0.05)(\mathbf{q}^2 + 0.0001). \quad (70)$$

Note that the NMP zero lies between the two unstable poles. Thus, in order to stabilize this plant, the controller must be unstable. RCAC places five closed-loop poles near the locations of the roots of D_p, as shown in Figure 27. Note that the controller converges to an unstable configuration and the spectral radius of the closed-loop system at step $k = 20$ is less than 1. ∎
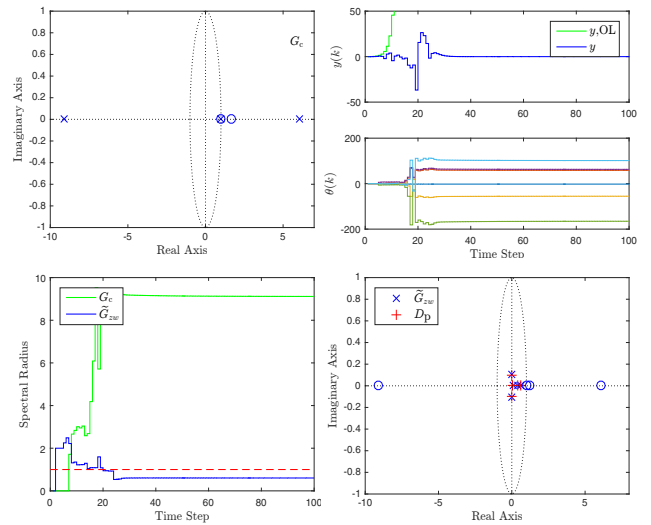

Fig. 27. Example 22: Step disturbance rejection for an unstably stabilizable plant. RCAC places five closed-loop poles near the locations of the roots of D_p. Note that the controller becomes unstable after a few steps and the closed-loop system is stabilized at step $k = 20$. The closed-loop poles and zeros are shown at step $k = 100$.

B. Harmonic Disturbance Rejection

In this section we consider unit-amplitude harmonic disturbance rejection, where the disturbance consists of two sinusoids with frequencies $\omega_1 = \frac{\pi}{8}$ rad/sample and $\omega_2 = \frac{\pi}{12}$ rad/sample. We consider various cases where y and z may be equal and where w and u may be matched.

Example 23. *Harmonic disturbance rejection with $y = z$ and with w matched with u.* Consider the asymptotically stable, NMP plant with $y = z$ and with w matched with u, shown in Figure 28. We use the FIR target model 21, and set $n_\mathrm{c} = 10$ and $R_\theta = 10^{-10}$. ∎
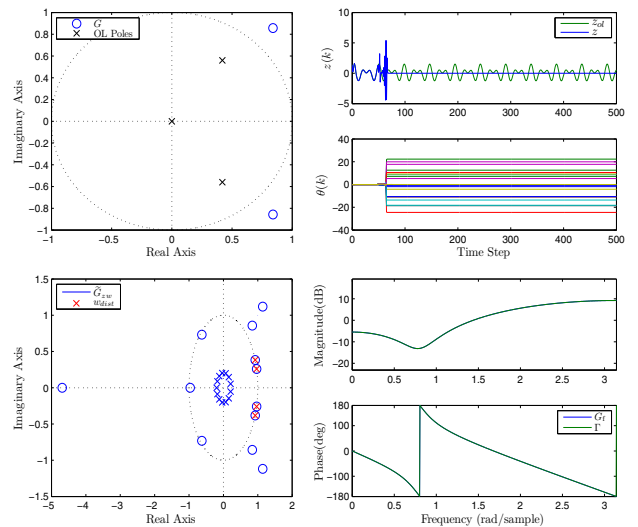

Fig. 28. Example 23: Harmonic disturbance rejection with $y = z$ and with w matched with u. RCAC places controller poles at the two disturbance frequencies, and $\widetilde{G}_{zw}$ is asymptotically stable. The frequency response of Γ matches the frequency response of G_f.

Example 24. *Harmonic disturbance rejection with $y \neq z$ and with w not matched with u.* Consider the asymptotically stable, NMP plant with $y \neq z$ and with w not matched with u, shown in Figure 29. We set $R_\theta = 10^{-10}$, $n_c = 10$, and $G_f(\mathbf{q}) = \frac{0.7708(\mathbf{q}^2 - 1.179\mathbf{q} + 1.011)}{\mathbf{q}^3}$, where the numerator contains H_d and the NMP zeros of G_{zu}. ∎
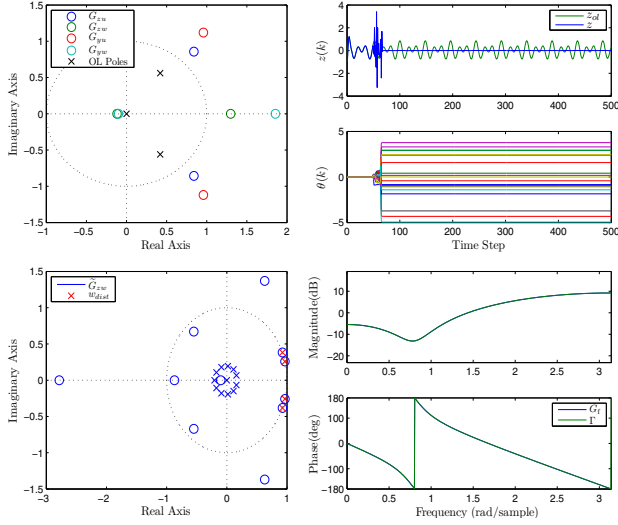

Fig. 29. Example 24: Harmonic disturbance rejection with $y \neq z$ and with w not matched with u. Only the NMP zeros of G_{zu} are modeled. RCAC places controller poles at the two disturbance frequencies, and $\widetilde{G}_{zw}$ is asymptotically stable. The frequency response of Γ matches the frequency response of G_f.

C. Broadband Disturbance Rejection

In this section we consider broadband disturbance rejection where the disturbance is zero-mean Gaussian white noise. We compare the closed-loop performance of RCAC to high-authority LQG without sensor noise. Sensor noise is considered in Section VI.

1) Matching high-authority LQG closed-loop performance: The closed-loop poles of high-authority LQG control without sensor noise are discussed in the Appendix. We attempt to match the closed-loop performance of high-authority LQG with RCAC by using $n_c = n$ and setting the pole locations in G_f to coincide with the high-authority LQG closed-loop poles. However, we show that this causes RCAC to place extra poles at the minimum-phase zeros of G_{zu}. We also show that RCAC can match the closed-loop performance of high-authority LQG by omitting the minimum-phase zeros of G_{zu}. Specifically, we choose

$$G_f(\mathbf{q}) = \frac{H_d N_{zu,\mathrm{u}} \mathbf{q}^m}{N_{zu,\mathrm{u}}(1/\mathbf{q}) N_{yw,\mathrm{s}}(\mathbf{q}) N_{yw,\mathrm{u}}(\mathbf{q}^{-1})}, \qquad (71)$$

where m is chosen such that the relative degree of G_f is in accordance with the relative degree of G_{zu}.

Example 25. *RCAC for the adaptive standard problem with $y = z$ and with w matched with u.* Consider the Lyapunov-stable NMP plant

$$G(\mathbf{q}) = \frac{(\mathbf{q} - 0.5)(\mathbf{q}^2 - 1.92\mathbf{q} + 1.44)}{(\mathbf{q} - 1)(\mathbf{q} - 0.9)(\mathbf{q}^2 - 1.62\mathbf{q} + 0.81)}, \qquad (72)$$

where the NMP zeros are complex. We set $n_c = n$ and use the high-authority LQG target model (71). RCAC places the closed-loop poles near the high-authority LQG closed-loop poles and approximates the closed-loop frequency response of high-authority LQG, as shown in Figure 30. ∎
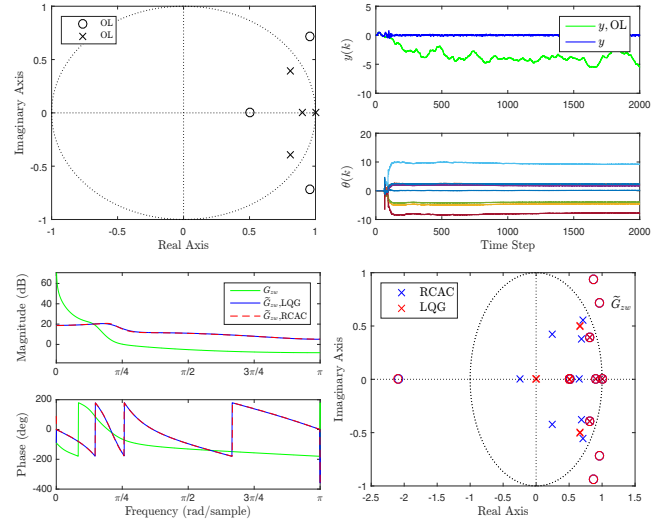

Fig. 30. Example 25: RCAC for the adaptive standard problem using the high-authority LQG target model (71). RCAC places the closed-loop poles near the high-authority LQG closed-loop poles and approximates the closed-loop frequency response of high-authority LQG. The frequency-response plots and closed-loop poles and zeros are shown at step $k = 10^4$.

Example 26. *RCAC for the adaptive standard problem with $y \neq z$, and with w not matched with u.* Consider the asymptotically stable plant

$$A = \begin{bmatrix} 0 & 1 & 0 & 0 \\ 0 & 0 & -0.4482 & 1.1491 \\ 0 & 0 & 0.81 & 1 \\ 0 & 0 & -0.1539 & 0.81 \end{bmatrix}, \ B = \begin{bmatrix} 0 \\ 0 \\ 0 \\ 1 \end{bmatrix}, \quad (73)$$

$$D_1 = \begin{bmatrix} 0.7343 \\ -0.1655 \\ -0.6579 \\ -0.0230 \end{bmatrix}, \ D_0 = E_2 = 0, \ D_2 = E_0 = 0, \quad (74)$$

$$C = [0.5754 \quad -0.5819 \quad 0.3479 \quad 0.4574], \qquad (75)$$

$$E_1 = [0.2608 \quad -0.7079 \quad -0.2385 \quad 0.6116], \qquad (76)$$

where G_{zu}, G_{yu}, and G_{yw} are NMP, and G_{zw} is minimum phase. We set $n_c = n$ and use the high-authority LQG target model (71). RCAC places the closed-loop poles near the high-authority LQG closed-loop poles and approximates the closed-loop frequency response of high-authority LQG, as shown in Figure 31. ∎

2) Matching high-authority LQG closed-loop performance with minimal modeling information: In LQG control,
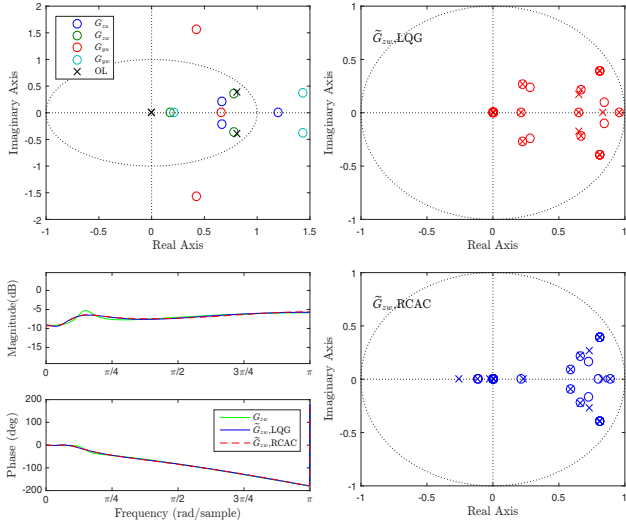
Fig. 31. Example 26: RCAC for the adaptive standard problem, with the high-authority LQG target model (71). RCAC places the closed-loop poles near the high-authority LQG closed-loop poles and approximates the closed-loop frequency response of high-authority LQG. The frequency-response plots and closed-loop poles and zeros are shown at step $k = 10^5$.
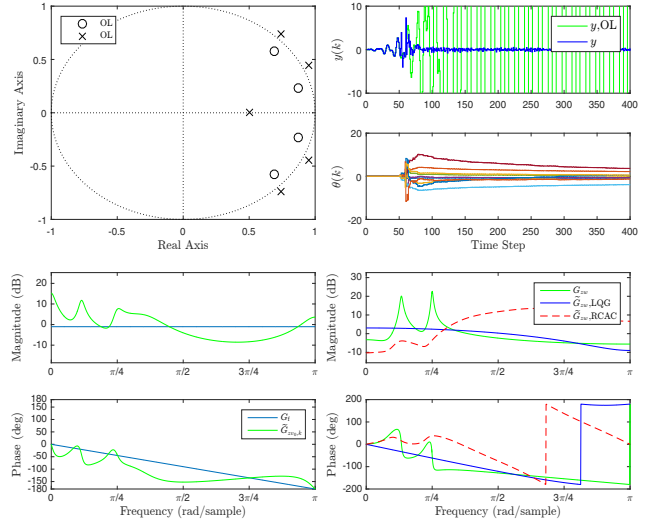

Fig. 32. Example 27: RCAC for the adaptive standard problem with $n_c = n$, using the FIR target model (20). RCAC does not approximate the closed-loop frequency response of high-authority LQG. In addition, the frequency response of Γ does not approximate the frequency response of G_f at low frequencies. The frequency-response plots are shown at step $k = 10^5$.
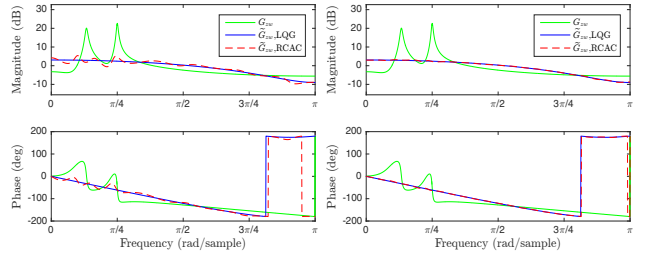

Fig. 33. Example 27: RCAC for the adaptive standard problem with $n_c = 10$ (left plots) and $n_c = 20$ (right plots), using the FIR target model (20) in both cases. RCAC approximates the closed-loop frequency response of high-authority LQG. In addition, the frequency response of Γ approximates the frequency response of G_f. Note that RCAC approximates the frequency response of high-authority LQG more closely as n_c is increased from 10 to 20. The frequency-response plots are shown at step $k = 10^5$.

the controller order is equal to the order of the plant. In this section, we show that, for sufficiently large $n_c > n$, RCAC approximates the performance of high-authority LQG using the FIR target models (20) and (21), which use knowledge of d_{zu}, $H_{d_{zu}}$, and the NMP zeros of G_{zu}.

Example 27. *RCAC for the adaptive standard problem with $y = z$ and with w matched with u.* Consider the unstable, minimum-phase plant

$$G(\mathbf{q}) = \frac{(\mathbf{q}^2 - 1.739\mathbf{q} + 0.81)(\mathbf{q}^2 - 1.379\mathbf{q} + 0.81)}{(\mathbf{q} - 0.5)(\mathbf{q}^2 - 1.9\mathbf{q} + 1.1)(\mathbf{q}^2 - 1.485\mathbf{q} + 1.1)},$$

(77)

where G_{zu}, G_{zw}, G_{yu}, and G_{yw} are minimum phase. We set $n_c = n = 5$, and we use the FIR target model (20). RCAC does not approximate the closed-loop frequency response of high-authority LQG, as shown in Figure 32. However, by using (71), RCAC approximates the closed-loop frequency response of LQG with $n_c = n$ (not shown).

Next, we increase n_c from $n_c = 5$ to $n_c = 10$ and again to $n_c = 20$. In both cases RCAC approximates the closed-loop frequency response of LQG, as shown in Figure 33. Note that RCAC approximates the frequency response of high-authority LQG more closely as n_c is increased from 10 to 20. ∎

Example 28. *RCAC for the adaptive standard problem with $y \neq z$ and with w not matched with u.* Consider the asymptotically stable plant

$$A = \begin{bmatrix} 0.855 & 1 & 0 & 0 & 0 \\ -0.1715 & 0.855 & -0.4266 & -0.3607 & 0.4952 \\ 0 & 0 & 0.5 & -0.5072 & 0.6964 \\ 0 & 0 & 0 & 0.6716 & 1 \\ 0 & 0 & 0 & -0.4514 & 0.6716 \end{bmatrix},$$

(78)

$$B = \begin{bmatrix} 0 \\ 0 \\ 0 \\ 0 \\ 1 \end{bmatrix}, \quad D_1 = \begin{bmatrix} -0.6269 \\ 0.3985 \\ -0.3306 \\ 0.4415 \\ 0.3794 \end{bmatrix},$$

(79)

$$C = [0.7298 \quad -0.3954 \quad -0.3605 \quad 0.4003 \quad 0.1447],$$

(80)

$$E_1 = [0.1717 \quad 0.3351 \quad -0.5294 \quad -0.4476 \quad 0.6145],$$

(81)

$$D_0 = E_2 = 0, \quad D_2 = E_0 = 0,$$

(82)

where G_{zu}, G_{zw}, G_{yu}, and G_{yw} are NMP. We set $n_c = 2n = 10$, and we use the FIR target model (21) without knowledge of $\widetilde{D}_{HA}$. In this case RCAC approximates the closed-loop frequency response of high-authority LQG, as shown in Figure 34. ■
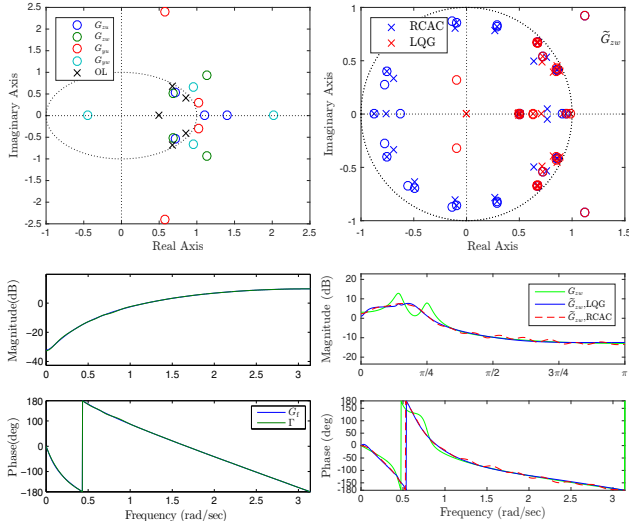

Fig. 34. Example 28: RCAC for the adaptive standard problem with $n_c = 10$. RCAC approximates the closed-loop frequency response of high-authority LQG. In addition, the frequency response of Γ approximates the frequency response of G_f. The frequency-response plots are shown at step $k = 10^5$.

Example 29. *RCAC for the adaptive standard problem with $y = z$ and with w matched with u.* We reconsider the Lyapunov-stable plant (72) in Example 25, and we let w be nonzero-mean white noise with mean 0.1. We set $n_c = 5n = 20$, and we use the FIR target model (21) without knowledge of $\widetilde{D}_{HA}$. RCAC approximates the closed-loop frequency response of high-authority LQG except at DC due to the internal model needed to reject the nonzero-mean disturbance, which is evident in the form of the notch at DC, as shown in Figure 35. ■

Example 30. *Harmonic command following and stochastic disturbance rejection for the adaptive servo problem.* Consider the asymptotically stable plant

$$G(\mathbf{q}) = \frac{(\mathbf{q}^2 - 1.7\mathbf{q} + 0.785)(\mathbf{q}^2 - 1.4\mathbf{q} + 0.85)}{(\mathbf{q} - 0.5)(\mathbf{q}^2 - 1.8\mathbf{q} + 0.97)(\mathbf{q}^2 - 1.4\mathbf{q} + 0.98)}, \tag{83}$$

where G is minimum phase. Let r be the harmonic command $r(k) = \cos \omega k$, where $\omega = 0.8$ rad/sample, and let $v = 0$. We set $n_c = 8n = 40$, and we use the FIR target model (20). RCAC follows the harmonic command and approximates the closed-loop frequency response of high-authority LQG except at the command frequency due to the internal model, which is evident in the form of the notch at the command frequency, as shown in Figure 36. ■
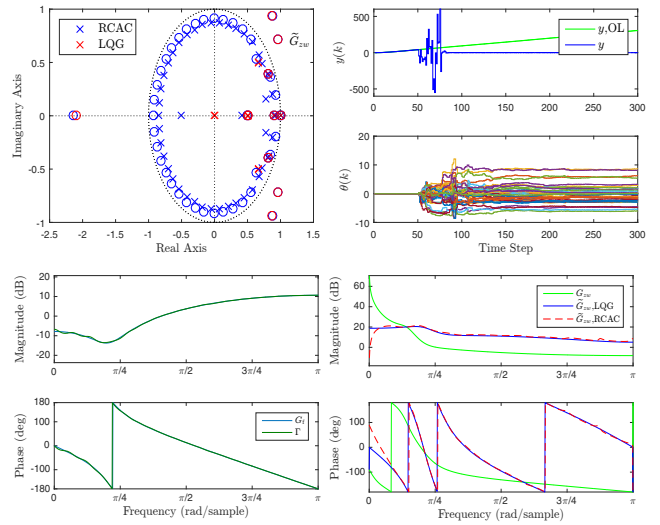

Fig. 35. Example 29: RCAC for the adaptive standard problem with $n_c = 5n = 20$. RCAC approximates the closed-loop frequency response of high-authority LQG except at DC due to the internal model needed to reject the step disturbance. The internal model is evident in the form of the notch at DC corresponding to the closed-loop zero at 1. In addition, the frequency response of Γ approximates the frequency response of G_f. The frequency-response plots and closed-loop poles and zeros are shown at step $k = 10^5$.

Fig. 36. Example 30: Command following and stochastic disturbance rejection for the adaptive servo problem with $n_c = 8n = 40$. RCAC approximates the closed-loop frequency response of high-authority LQG except at the command frequency due to the internal model. The internal model is evident in the form of the notch at the command frequency corresponding to the closed-loop zeros on the unit circle. The frequency-response plots and closed-loop poles and zeros are shown at step $k = 10^5$.

Example 31. *Step command following and stochastic disturbance rejection for the adaptive servo problem.* Consider

the asymptotically stable plant

$$A = \begin{bmatrix} 0.861 & 1 & 0 & 0 & 0 \\ -0.1612 & 0.861 & -0.3095 & -0.3417 & 0.6314 \\ 0 & 0 & 0.6718 & 1 & 0 \\ 0 & 0 & -0.4512 & 0.6718 & 0.7302 \\ 0 & 0 & 0 & 0 & 0.5 \end{bmatrix},$$

(84)

$$B = \begin{bmatrix} 0 \\ 0 \\ 0 \\ 0 \\ 1 \end{bmatrix}, \quad \bar{D}_1 = \begin{bmatrix} 0.5537 \\ 0.0603 \\ -0.5457 \\ 0.5596 \\ -0.2806 \end{bmatrix}, \quad \bar{D}_2 = 0, \quad \bar{D}_0 = 0,$$

(85)

$$\bar{C} = [0.2312 \quad 0.3910 \quad -0.3527 \quad -0.3894 \quad 0.7195],$$

(86)

where G_u and G_d are minimum phase. Let r be a unit step command, and let $v = 0$. We set $n_c = 4n = 20$, and we use the FIR target model (20). RCAC follows the step command and approximates the closed-loop frequency response of high-authority LQG except at DC due to the internal model, which is evident in the form of the notch at DC, as shown in Figure 37. ∎
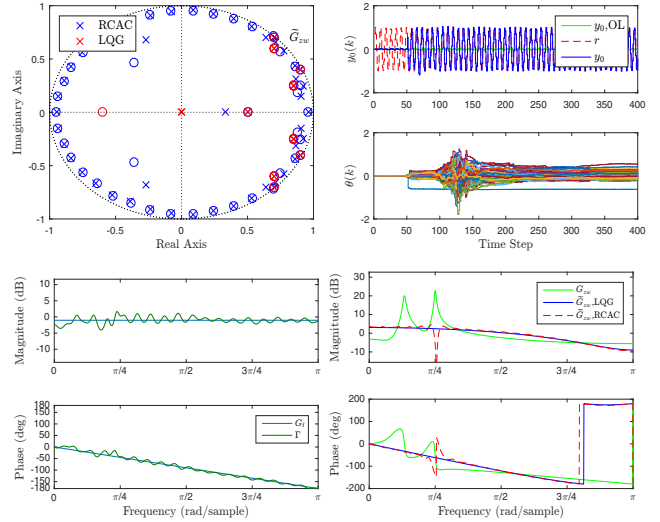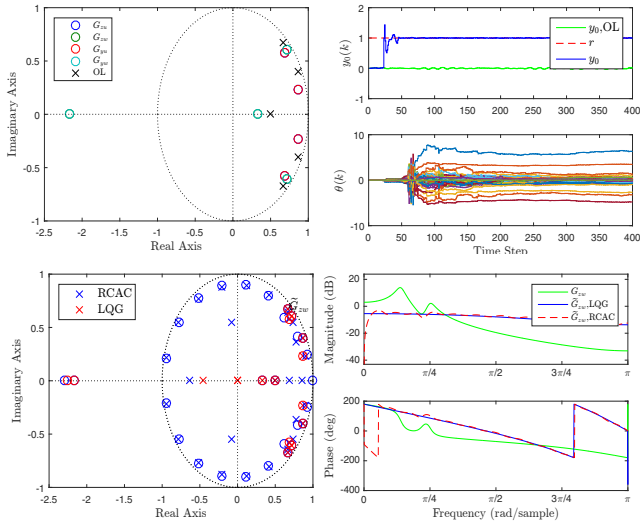

Fig. 37. Example 31: Command following and stochastic disturbance rejection for the adaptive servo problem with $n_c = 4n = 20$. RCAC approximates the closed-loop frequency response of high-authority LQG except at DC due to the internal model. The internal model is evident in the form of the notch at DC corresponding to the closed-loop zero at 1. The frequency-response plots and closed-loop poles and zeros are shown at step $k = 10^5$.

VI. EFFECT OF SENSOR NOISE

In all examples considered so far in this paper, the measurement y is not corrupted by noise. In contrast, the examples in this section consider the adaptive servo problem where the sensor noise v is stochastic.

Example 32. *Pole placement for the adaptive servo problem with sensor noise.* Consider the asymptotically stable,

minimum-phase plant

$$G(\mathbf{q}) = \frac{\mathbf{q}^2 - 1.4\mathbf{q} + 0.85}{(\mathbf{q} - 0.99)(\mathbf{q}^2 - 1.6\mathbf{q} + 0.89)}.$$

(87)

Let r be a unit step command, and let $d = v = 0$. We set $R_\theta = 10^{-10}$ and $n_c = 4$. To place four closed-loop poles at ± 0.5 and $\pm 0.6\jmath$, we use the IIR target model (22) with

$$D_{\mathrm{p}}(\mathbf{q}) = (\mathbf{q} + 0.5)(\mathbf{q} - 0.5)(\mathbf{q}^2 + 0.36).$$

(88)

RCAC places closed-loop poles near the locations of the roots of D_{p}. Now, let v be nonzero-mean Gaussian white noise with mean 0.5 and standard deviation σ. For $\sigma = 0.01$, RCAC places closed-loop poles near the locations of the roots of D_{p}. However, for $\sigma = 0.1$, RCAC fails to place closed-loop poles near the locations of the roots of D_{p}. However, in both cases, the closed-loop system is asymptotically stable at step $k = 100$. Asymptotic stability is also obtained at step $k = 100$ for $\sigma = 1$ and $\sigma = 10$ (not shown). ∎

Fig. 38. Example 32: Pole placement for the adaptive servo problem without sensor noise (upper plots), as well as with sensor noise v with standard deviation $\sigma = 0.01$ (middle plots) and $\sigma = 0.1$ (lower plots). For $\sigma = 0.01$, RCAC places closed-loop poles near the locations of the roots of D_{p}. However, for $\sigma = 0.1$, RCAC fails to place closed-loop poles near the locations of the roots of D_{p}. However, in both cases, the closed-loop system is asymptotically stable at step $k = 100$. The closed-loop poles and zeros are shown at step $k = 100$.

Example 33. *Pole placement for the adaptive servo problem with sensor noise.* Consider the unstable, minimum-

phase plant

$$G(\mathbf{q}) = \frac{\mathbf{q}^2 - 1.4\mathbf{q} + 0.85}{(\mathbf{q} - 1.1)(\mathbf{q}^2 - 1.8\mathbf{q} + 1.06)}. \quad (89)$$

Let r be the harmonic command $r(k) = \cos \omega k$, where $\omega = 0.3$ rad/sample, and let $d = v = 0$. We set $R_\theta = 10^{-10}$ and $n_c = 6$. To place four closed-loop poles at 0, 0.5, and $\pm 0.1\jmath$, we use the IIR target model (22) with

$$D_\mathrm{p}(\mathbf{q}) = \mathbf{q}^4 - 0.5\mathbf{q}^3 + 0.01\mathbf{q}^2 - 0.005\mathbf{q}. \quad (90)$$

RCAC places closed-loop poles near the locations of the roots of D_p. Now let v be zero-mean Gaussian white noise with standard deviation σ. For $\sigma = 0.1$, RCAC fails to place closed-loop poles near the locations of the roots of D_p, but stabilizes the system at step $k = 500$. For $\sigma = 0.2$, RCAC fails to place closed-loop poles near the locations of the roots of D_p, and the closed-loop system is unstable at step $k = 500$. ■
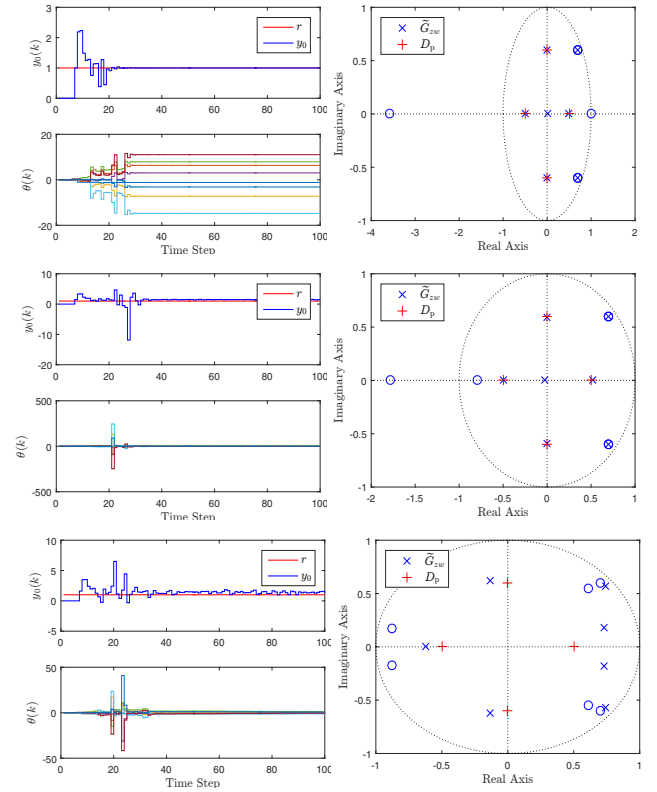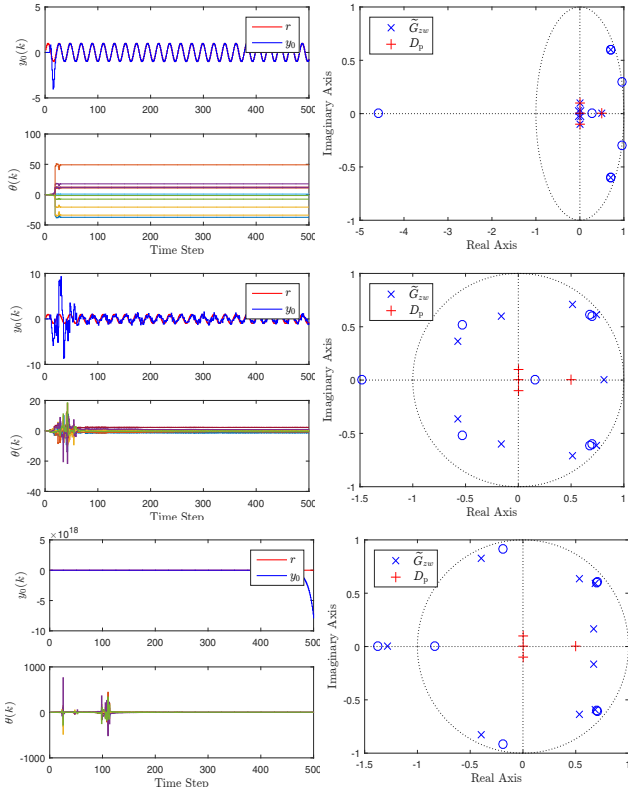

Fig. 39. Example 33: Pole placement for the adaptive servo problem without sensor noise (upper plots), as well as with zero-mean Gaussian white sensor noise v, with $\sigma = 0.1$ (middle plots) and $\sigma = 0.2$ (lower plots). In the case where $v = 0$, RCAC places closed-loop poles near the locations of the roots of D_p. For $\sigma = 0.1$, RCAC fails to place closed-loop poles near the locations of the roots of D_p, but stabilizes the system. However, for $\sigma = 0.2$, RCAC fails to place closed-loop poles near the locations of the roots of D_p, and the closed-loop system is unstable at step $k = 500$. The closed-loop poles and zeros are shown at step $k = 500$.

Example 34. *Stabilization for the adaptive servo problem with sensor noise.* Consider the unstable, NMP plant from Example 22 given by (69), for which stabilization requires

an unstable controller. Let $r = 0$ and $d = 0$, and let v be zero-mean Gaussian white noise with standard deviation $\sigma = 0.05$. We use the FIR target model (21), and set $R_\theta = 10^{-20}$ and $n_c = 3$. RCAC stabilizes (69) in the presence of sensor noise, as shown in Figure 40. For $\sigma = 0.15$, the closed-loop system is unstable at step $k = 100$. ■
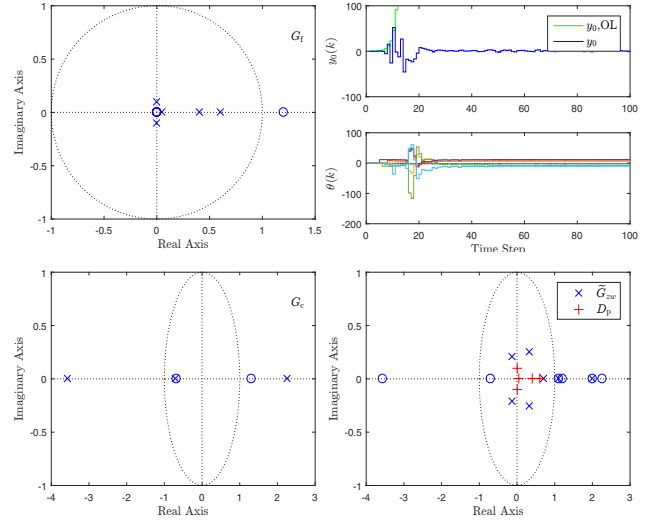

Fig. 40. Example 34: Stabilization for the adaptive servo problem with sensor noise. $\widetilde{G}_{zw}$ is asymptotically stable at step $k = 100$. Although RCAC stabilizes the unstable plant in the presence of sensor noise, RCAC does not place closed-loop poles at the locations of the poles of D_p. The closed-loop poles and zeros are shown at step $k = 100$.

Example 35. *Stochastic disturbance rejection for the adaptive servo problem with sensor noise.* Consider the asymptotically stable, minimum-phase plant

$$G(\mathbf{q}) = \frac{(\mathbf{q}^2 - 1.6\mathbf{q} + 0.73)(\mathbf{q}^2 - 1.44\mathbf{q} + 0.81)}{(\mathbf{q} - 0.9)(\mathbf{q} - 0.95)^2(\mathbf{q}^2 - 1.3\mathbf{q} + 0.845)}. \quad (91)$$

Let v be zero-mean Gaussian white sensor noise with standard deviation $\sigma = 1$. We set $k_\mathrm{w} = 50$, $R_\theta = 10^{-20}$, $R_u = 0$, $n_c = 2n = 10$, and we use the FIR target model (20). RCAC does not approximate the closed-loop frequency response of high-authority LQG. However, RCAC approximates the closed-loop frequency response of LQG for $V_2 = 1$, as shown in Figure 41. ■

Example 36. *Step command following and stochastic disturbance rejection for the adaptive servo problem with*
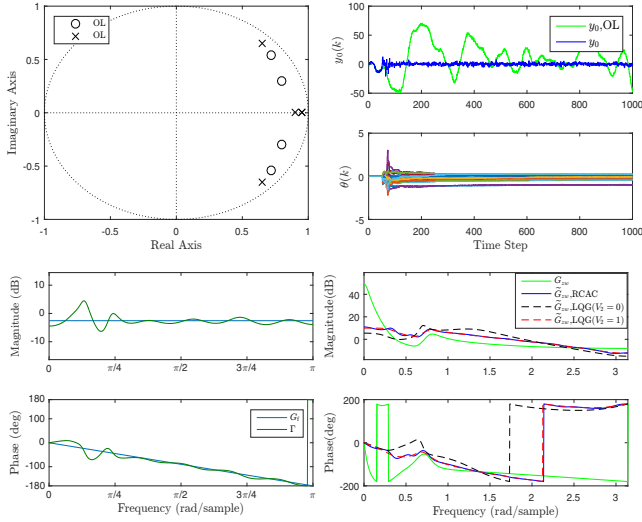
Fig. 41. Example 35: Stochastic disturbance rejection for the adaptive servo problem with zero-mean Gaussian white sensor noise. RCAC approximates the closed-loop frequency response of LQG for $V_2 = 1$. In addition, the frequency response of Γ approximates the frequency response of G_f. The frequency-response plots are shown at step $k = 10^5$.
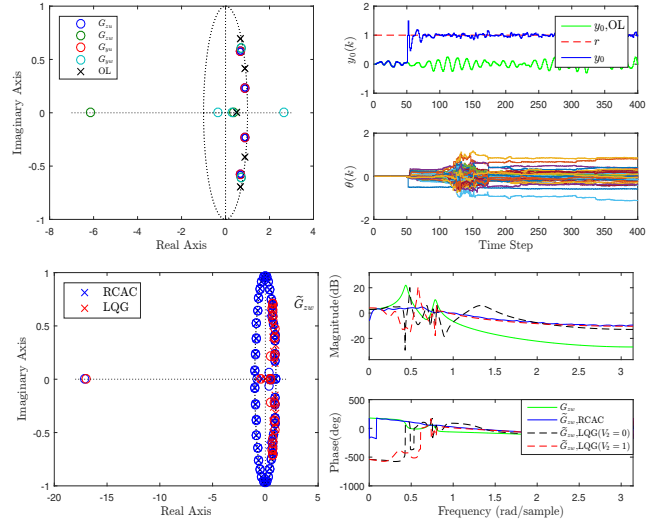

Fig. 42. Example 36: Command following and stochastic disturbance rejection for the adaptive servo problem with zero-mean Gaussian white sensor noise. RCAC approximates the closed-loop frequency response of LQG for $V_2 = 1$ except at DC due to the internal model. The internal model is evident in the form of the notch at DC corresponding to the closed-loop zero at 1. This example shows that RCAC approximates the closed-loop frequency response of LQG in the presence of sensor noise. The frequency-response plots and closed-loop poles and zeros are shown at step $k = 10^5$.

sensor noise. Consider the asymptotically stable plant

$$A = \begin{bmatrix} 0.8882 & 1 & 0 & 0 & 0 \\ -0.1715 & 0.8882 & -0.3624 & -0.3238 & 0.6679 \\ 0 & 0 & 0.693 & 1 & 0 \\ 0 & 0 & -0.4802 & 0.693 & 0.7276 \\ 0 & 0 & 0 & 0 & 0.5 \end{bmatrix},$$
(92)

$$B = \begin{bmatrix} 0 \\ 0 \\ 0 \\ 0 \\ 1 \end{bmatrix}, \quad D_1 = \begin{bmatrix} 0.5537 \\ 0.0603 \\ -0.5457 \\ 0.5596 \\ -0.2806 \end{bmatrix}, \quad \bar{D}_2 = 0, \quad \bar{D}_0 = 0,$$
(93)

$$\bar{C} = [0.2158 \quad 0.4234 \quad -0.3861 \quad -0.3449 \quad 0.7115],$$
(94)

where G_u and G_d are minimum phase. Let r be a unit step command, and let v be zero-mean Gaussian white noise with standard deviation $\sigma = 0.025$. We set $n_c = 8n = 40$, and we use the FIR target model (20). RCAC follows the step command and approximates the closed-loop frequency response of LQG except at DC due to the internal model, which is evident in the form of the notch at DC, as shown in Figure 42. This example shows that RCAC approximates the closed-loop frequency response of LQG in the presence of sensor noise, that is, the closed-loop frequency response of LQG for $V_2 = 1$. ∎

VII. ROBUSTNESS TO MODEL ERROR

As shown by the construction of G_f given by (20), (21), (22), and (23), the modeling information required by RCAC is d_{zu}, $H_{\mathrm{d}_{zu}}$, and the NMP zeros of G_{zu}. In this section we investigate the effect of modeling errors in this data.

Example 37. *Erroneous* d_{zu} *for the adaptive servo problem.* Consider the asymptotically stable, minimum-phase plant

$$G(\mathbf{q}) = \frac{\mathbf{q} - 0.95}{(\mathbf{q} - 0.85)(\mathbf{q}^2 - 1.5\mathbf{q} + 0.985)}.$$
(95)

Let r be the harmonic command $r(k) = \cos\omega k$, where $\omega = 0.15$ rad/sample, and let $d = v = 0$. We set $R_\theta = 10$ and $n_c = 6$. For G given by (95), $\mathrm{d}_{zu} = 2$. We use the FIR target model (20), but with d_{zu} replaced by $\hat{\mathrm{d}}_{zu}$, where $\hat{\mathrm{d}}_{zu}$ is an estimate of d_{zu}. Figure 43 shows the command-following performance for $\hat{\mathrm{d}}_{zu} = 1$, $\hat{\mathrm{d}}_{zu} = 3$, and $\hat{\mathrm{d}}_{zu} = 4$. For $\hat{\mathrm{d}}_{zu} = 3$ and $\hat{\mathrm{d}}_{zu} = 4$, RCAC follows the harmonic command. For $\hat{\mathrm{d}}_{zu} = 1$, RCAC does not follow the harmonic command, and the plant output y_0 diverges. RCAC follows the command for $2 \leq \hat{\mathrm{d}}_{zu} \leq 4$. Moreover, by using $R_u = z^2$, RCAC follows the command for $1 \leq \hat{\mathrm{d}}_{zu} \leq 10$. This example shows that RCAC is robust to over-estimates of d_{zu}, but is less robust to under-estimates of d_{zu}. Note that $\hat{d}_{zu} > d_{zu}$ accounts for an unmodeled time delay of $\hat{d}_{zu} - d_{zu}$ steps in the sense that, if the plant experiences an unmodeled time delay of $\hat{d}_{zu} - d_{zu}$ steps, then $\hat{d}_{zu}$ is the true relative degree. The next example considers time delay explicitly. ∎

Example 38. *Unmodeled time delay for the adaptive servo problem.* Consider the asymptotically stable,
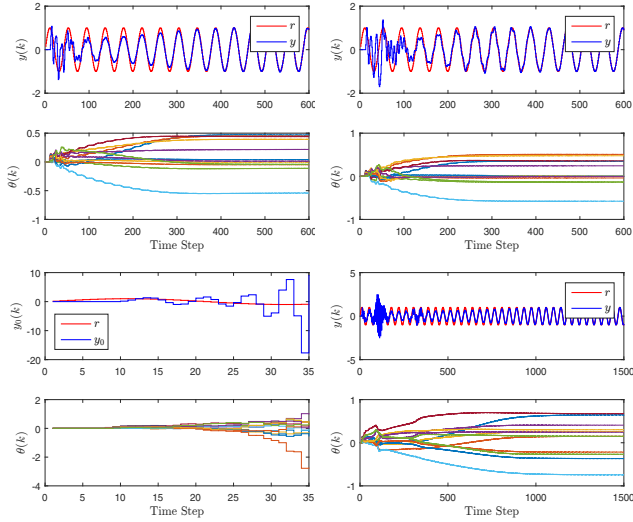
Fig. 43. Example 37: Effect of erroneous relative degree on command-following performance for the adaptive servo problem. For $\hat{d}_{zu} = 3$ (upper left) and $\hat{d}_{zu} = 4$ (upper right), RCAC follows the harmonic command. For $\hat{d}_{zu} = 1$ (lower left), RCAC does not follow the harmonic command, and the plant output y_0 diverges. However, by using the performance-dependent control weighting $R_u = z^2$ (lower right), RCAC follows the harmonic command, although the transient response is poor. This example shows that RCAC is robust to over-estimates of d_{zu}, but is less robust to under-estimates of d_{zu}.

minimum-phase plant $G = G_{\mathrm{TD}}G_0$, where

$$G_{\mathrm{TD}}(\mathbf{q}) \triangleq \mathbf{q}^{-k_{\mathrm{d}}}, \quad G_0(\mathbf{q}) = \frac{\mathbf{q} - 0.95}{(\mathbf{q} - 0.85)(\mathbf{q}^2 - 1.6\mathbf{q} + 0.89)}, \tag{96}$$

and G_{TD} represents an unmodeled time delay of k_{d} steps. Let r be the harmonic command $r(k) = \cos\omega k$, where $\omega = 0.35$ rad/sample, and let $d = v = 0$. We set $R_\theta = 0.03$, $R_u = z^2$, and $n_{\mathrm{c}} = 10$. Since G_{TD} is unmodeled, we use the FIR target model (20) based on G_0. Figure 44 shows the command-following error e_0 for $k_{\mathrm{d}} = 1$, $k_{\mathrm{d}} = 2$, $k_{\mathrm{d}} = 3$, and $k_{\mathrm{d}} = 4$. RCAC follows the harmonic command in each case. ∎

Example 39. *Erroneous $H_{\mathrm{d}_{zu}}$ for the adaptive servo problem.* Consider the asymptotically stable, minimum-phase plant

$$G(\mathbf{q}) = \frac{(\mathbf{q} - 0.99)(\mathbf{q} - 0.90)}{(\mathbf{q} - 0.95)(\mathbf{q}^2 - 1.6\mathbf{q} + 0.89)}. \tag{97}$$

Let r be a unit step command, and let $d = v = 0$. We set $R_\theta = 10$ and $n_{\mathrm{c}} = 5$. We use the FIR target model (20) with H_{d} replaced by $\hat{H}_{\mathrm{d}}$, where $\hat{H}_{\mathrm{d}}$ is an estimate of the true value $H_{\mathrm{d}} = 1$. Figure 45 shows the command-following performance for $\hat{H}_{\mathrm{d}} = -1$, $\hat{H}_{\mathrm{d}} = 0.1$, and $\hat{H}_{\mathrm{d}} = 10$. RCAC follows the command for $\hat{H}_{\mathrm{d}_{zu}} = 0.1$ and $\hat{H}_{\mathrm{d}_{zu}} = 10$, but not for $\hat{H}_{\mathrm{d}} = -1$. This example shows that RCAC is robust to errors in the magnitude of the estimate of H_{d}, but is not robust to errors in the sign of the estimate of H_{d}. ∎

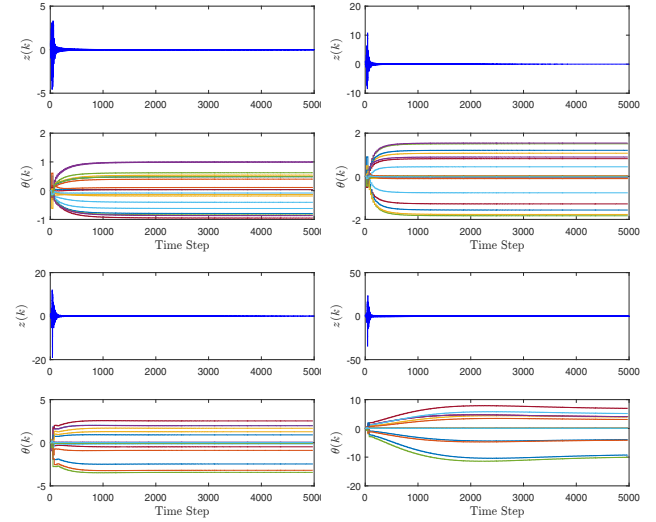**Example 40.** *Unmodeled NMP zero in G for the adaptive*

Fig. 44. Example 38: Unknown time delay for the adaptive servo problem. For $k_{\mathrm{d}} = 1$ (top left), $k_{\mathrm{d}} = 2$ (top right), $k_{\mathrm{d}} = 3$ (bottom left), and $k_{\mathrm{d}} = 4$ (bottom right). RCAC follows the harmonic command in each case.
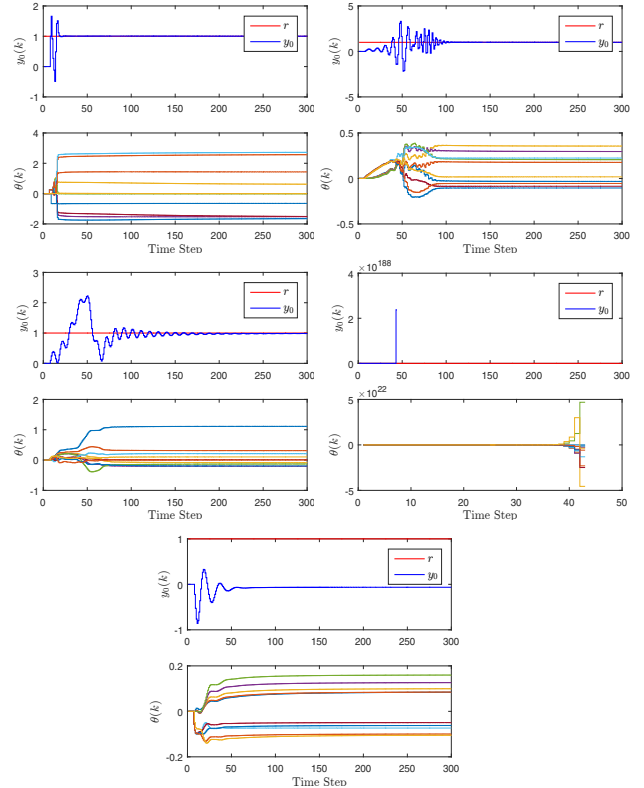

Fig. 45. Example 39: Effect of erroneous H_{d} on command-following performance for the adaptive servo problem. Command-following performance in for $\hat{H}_{\mathrm{d}} = H_{\mathrm{d}} = 1$ (top), $\hat{H}_{\mathrm{d}} = 0.1$ (middle left), $\hat{H}_{\mathrm{d}} = 10$ (middle right), $\hat{H}_{\mathrm{d}_{zu}} = -1$ (bottom left), and $\hat{H}_{\mathrm{d}_{zu}} = -1$ with performance-dependent control weighting $R_u = z^2$ (bottom right). RCAC follows the command for $\hat{H}_{\mathrm{d}} = 0.1$ and $\hat{H}_{\mathrm{d}} = 10$, however, note that the transient response degrades compared to $\hat{H}_{\mathrm{d}} = H_{\mathrm{d}}$. For $\hat{H}_{\mathrm{d}} = -1$, RCAC causes instability if $R_u = 0$, but the closed-loop remains asymptotically stable at step $k = 5000$ by using R_u (not shown). This example shows that RCAC is robust to errors in the magnitude of the estimate of H_{d}, but is not robust to errors in the sign of the estimate of H_{d}.

servo problem. Consider the Lyapunov-stable, NMP plant

$$G(\mathbf{q}) = \frac{(\mathbf{q} - 1.1)(\mathbf{q} - 0.9)}{(\mathbf{q} - 0.8)(\mathbf{q} - 0.95)(\mathbf{q} - 1)}. \tag{98}$$

Let r be a unit step command, and let $d = v = 0$. We set $R_\theta = 1$ and $n_c = 15$. We assume that the NMP zero of G is unmodeled, and we thus use the FIR target model (20) for minimum-phase plants. Figure 46 shows the command-following performance. Note that RCAC cancels the NMP zero of G_{zu} in order to match the frequency response of Γ to the frequency response of G_f. Because of unstable pole-zero cancellation, the output y_0 diverges. Next, we use the performance-dependent control weighting $R_u = z^2$. In this case, unstable pole-zero cancellation does not occur, and RCAC follows the command without knowledge of the unmodeled NMP zero. ∎
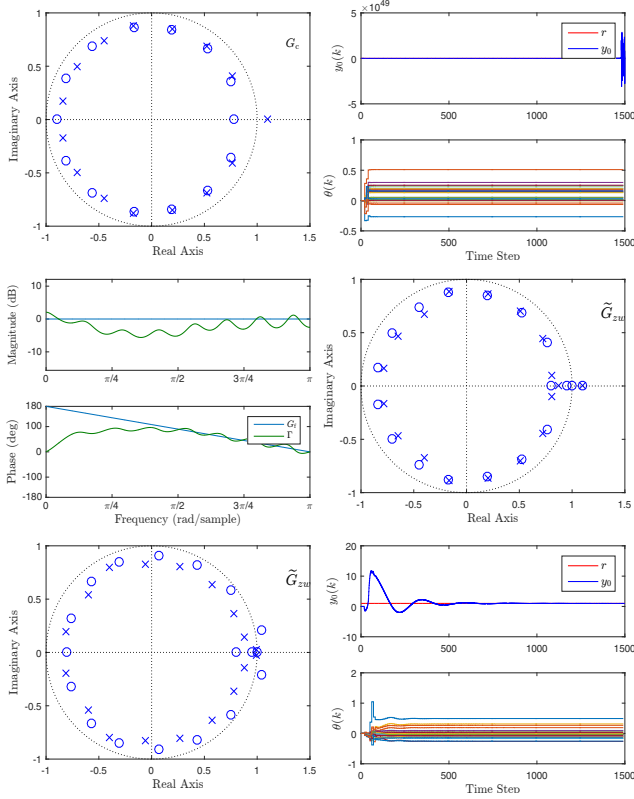

Fig. 46. Example 40: Unmodeled NMP zero in G_{zu} and unstable pole-zero cancellation for the adaptive servo problem. Since G_f does not capture the NMP zero of G_{zu}, unstable pole-zero cancellation occurs, and the closed-loop system is unstable. Using the performance-dependent control weighting $R_u = z^2$, unstable pole-zero cancellation does not occur, and RCAC follows the command without knowledge of the unmodeled NMP zero. The frequency-response plots and closed-loop poles and zeros are shown at step $k = 2000$.

Example 41. *Unmodeled NMP zero in G for the adaptive servo problem for unstable G.* Consider the unstable, NMP double integrator

$$G(\mathbf{q}) = \frac{\mathbf{q} - 1.15}{(\mathbf{q} - 1)^2}. \qquad (99)$$

Let r be the harmonic command $r(k) = \cos \omega k$, where $\omega = 0.55$ rad/sample, and let $d = v = 0$. We set $n_c = 10$, $R_\theta = 10^4$, and $R_u = z^2$. We assume that the NMP zero of G is unmodeled, and we thus use the FIR target model (20)

for minimum-phase plants. Figure 47 shows the command-following performance. As z becomes unbounded, the term $\sum_{i=1}^{k} \lambda^{k-i} \hat{\theta}^T \Phi_f^T(i) R_u(i) \Phi_f(i) \hat{\theta}$ in (24) dominates the remaining terms, and u converges to 0. Therefore, the closed-loop system reverts back to the unstable open-loop system, and RCAC does not follow the harmonic command. This example shows that RCAC is not robust to unmodeled NMP zeros for unstable systems, despite using the performance-dependent control weighting $R_u = z^2$. ∎
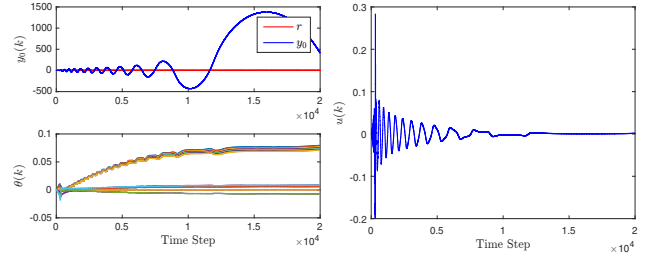

Fig. 47. Example 41: Unmodeled NMP zero in G for the adaptive servo problem. RCAC does not follow the harmonic command, and as z becomes unbounded, the closed-loop system tends to the unstable open-loop system. This example shows that RCAC is not robust to unmodeled NMP zeros for unstable systems, despite using the performance-dependent control weighting $R_u = z^2$.

Example 42. *Erroneous NMP-zero locations for the adaptive servo problem.* Consider the asymptotically stable, NMP plant

$$G(\mathbf{q}) = \frac{(\mathbf{q} - 0.85)(\mathbf{q} - 0.90)(\mathbf{q} - 1.1)}{(\mathbf{q} - 0.95)^2(\mathbf{q}^2 - 1.4\mathbf{q} + 0.98)}. \qquad (100)$$

Let r be the harmonic command $r(k) = \cos \omega k$, where $\omega = 0.4$ rad/sample, and let $d = v = 0$. We use the target model $G_f(\mathbf{q}) = \frac{H_{d_{zu}}(\mathbf{q} - 1.265)}{\mathbf{q}^2}$, where the estimate 1.265 of the NMP zero 1.1 is erroneous by 15%, and set $R_\theta = 30$ and $n_c = 8$. Figure 48 shows the command-following performance. In this example, the error in the NMP zero estimate can be increased to approximately 32% above the true value without causing instability. ∎
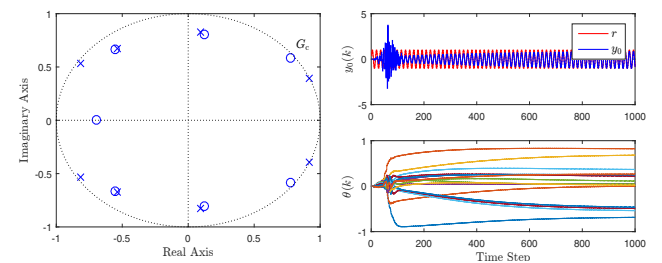

Fig. 48. Example 42: Erroneous NMP-zero locations for the adaptive servo problem. RCAC follows the command and develops an internal model of the command despite a 15% error in the estimate of the NMP zero used by the G_f. In this example, the error in the NMP zero estimate can be increased to approximately 32% above the true value without causing instability. The controller poles are shown at step $k = 1000$.

VIII. APPLICATION TO CONTROL SATURATION

We now investigate the performance of RCAC in the presence of control magnitude and rate saturation, as shown in Figure 49. The output of RCAC is the requested control $u_r(k)$, and the input to the plant is the actual control $u(k)$. In all examples, the regressor $\Phi(k)$ contains $u(k)$. This means that either the nonlinearity is known or its output is measured. The case where the nonlinearity is unknown and its output is not measured is considered in [21].
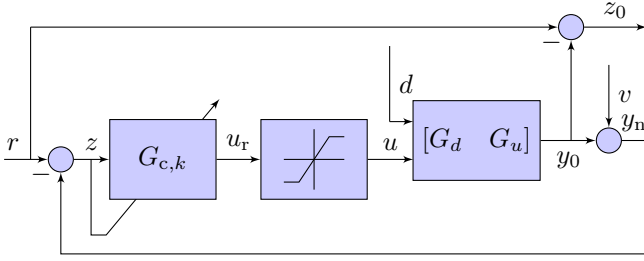

Fig. 49. Adaptive servo problem with control magnitude and rate saturation.

Example 43. *Magnitude saturation for the adaptive servo problem.* Consider the unstable, NMP double integrator

$$G(\mathbf{q}) = \frac{\mathbf{q} - 1.05}{(\mathbf{q} - 1)^2}. \tag{101}$$

Let r be the ramp command $r(k) = 0.1k$. We set $n_c = 12$, $R_\theta = 10^{-3}$, and we use the FIR target model (21). The control u is magnitude-saturated at ± 2. Figure 50 shows that RCAC follows the command despite the magnitude saturation. Next, u is magnitude-saturated at ± 0.5. In this case, RCAC cannot follow the ramp command, but the error remains bounded. ∎
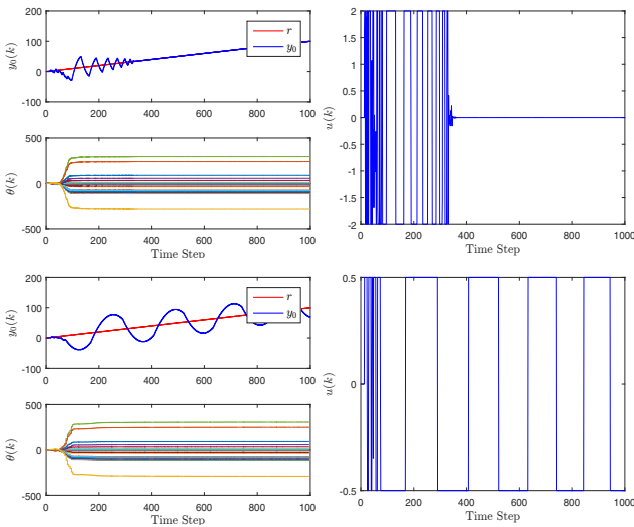

Fig. 50. Example 43: Magnitude saturation for the adaptive servo problem. RCAC follows the command despite the magnitude saturation. The performance degrades as the control magnitude saturation limits is decreased from 2.0 and 0.5. The command-following error e_0 diverges for a saturation limit of 0.05.

Example 44. *Control magnitude and rate saturation for the adaptive servo problem.* Consider the unstable, NMP double integrator (101). Let r be the ramp command $r(k) = 0.1k$. We set $n_c = 12$ and $R_\theta = 10^{-3}$, and we use the FIR target model (21). The control u is magnitude-saturated at ± 2 and rate-saturated at ± 1.5, which means that the one-step change in the control signal is magnitude-saturated at 1.5. Despite the magnitude and rate saturation, Figure 51 shows that RCAC follows the command, but more time is needed to reach zero error. Next, the rate saturation is decreased to ± 1. In this case, RCAC cannot follow the ramp command, and the command-following error e_0 diverges. ∎
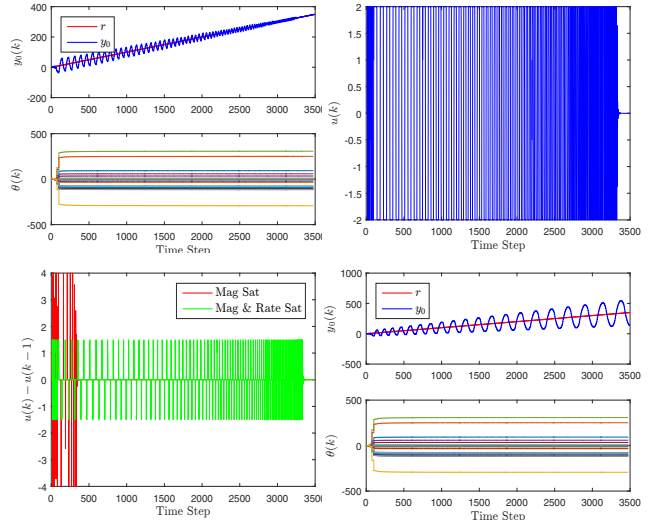

Fig. 51. Example 44: Control magnitude and rate saturation for the adaptive servo problem. Despite the magnitude and rate saturation, RCAC follows the command, but the time taken to reach zero error is longer than in the case where u is not saturated. In the case where the rate saturation is decreased to ± 1, RCAC cannot follow the ramp command, and the command-following error e_0 diverges.

Example 45. *Magnitude and rate saturation for the adaptive servo problem.* Consider the unstable, NMP triple integrator

$$G(\mathbf{q}) = \frac{(\mathbf{q} - 1.075)(\mathbf{q} - 0.95)}{(\mathbf{q} - 1)^3}. \tag{102}$$

Let r be the ramp command $r(k) = k$. We set $n_c = 10$, $R_\theta = 10^{-2}$, and $R_u = 0$, and we use the FIR target model (21). The control u is magnitude-saturated at ± 200 and rate-saturated at ± 160. Despite the magnitude and rate saturation, Figure 52 shows that RCAC follows the command. Note that this example demonstrates saturated control of the triple integrator using output feedback. In contrast, [45], [46] use full-state feedback. ∎

Example 46. *Magnitude saturation for the adaptive servo problem.* Consider the asymptotically stable, minimum-phase
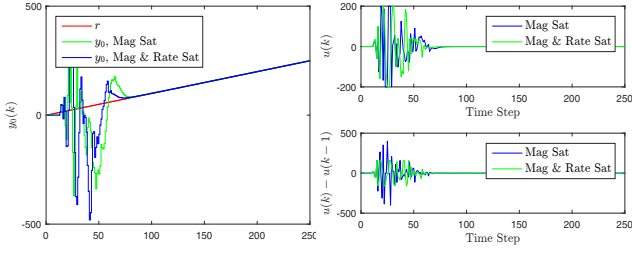
Fig. 52. Example 45: Magnitude and rate saturation for the adaptive servo problem. Despite the magnitude and rate saturation, RCAC follows the command.

Fig. 54. Example 46: Magnitude saturation for the adaptive servo problem. RCAC develops an internal model in the form of an integrator (not shown). Due to the magnitude saturation, the asymptotic error is nonzero. However, RCAC does not exhibit integrator windup.

plant from [47]

$$G(\mathbf{q}) = \frac{\mathbf{q}^2 - 0.4\mathbf{q} + 0.29}{(\mathbf{q}^2 - \mathbf{q} + 0.5)(\mathbf{q} - 0.9)}. \quad (103)$$

Let r be a square wave with unit amplitude and with period 1000 steps, and let $d = v = 0$. Consider the fixed-gain controller

$$G_{\mathrm{PI}}(\mathbf{q}) = 0.2 + \frac{0.02}{\mathbf{q} - 1}. \quad (104)$$

Figure 53 shows the command-following performance for G_{PI} with u unsaturated and with u magnitude-saturated at ± 0.03. Note that, in the case where u is magnitude-saturated, the asymptotic error is nonzero and the requested control u_{r} exhibits integrator windup. The windup causes phase lag in y_0 relative to the command. Next, we use RCAC with
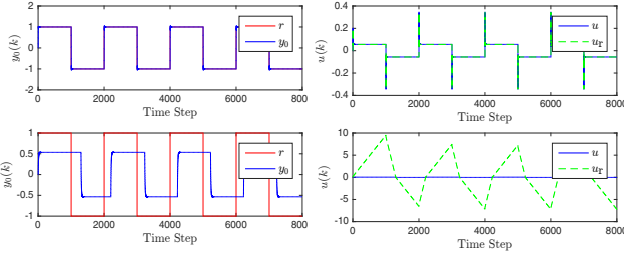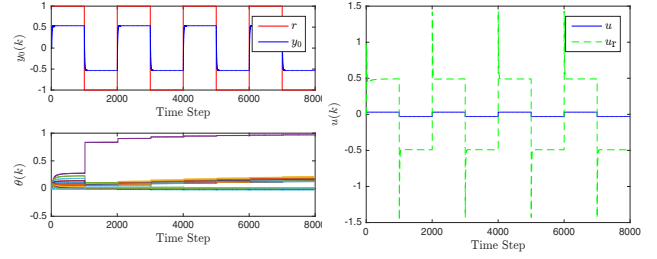

Fig. 53. Example 46: For unsaturated u (upper plots), G_{PI} follows the command, and the asymptotic error is zero. For u saturated at ± 0.03 (lower plots), the asymptotic error is nonzero, and the unsaturated control signal u_{r} exhibits integrator windup.

$n_{\mathrm{c}} = 10$, $R_\theta = 1$, and the FIR target model (20). The control u is magnitude-saturated at ± 0.03. Figure 54 shows the command-following performance. RCAC develops an internal model in the form of an integrator (not shown). Due to the magnitude saturation, the asymptotic error is nonzero. However, RCAC does not exhibit integrator windup, and y_0 remains in phase with r. ∎

Example 47. *Deadzone for the adaptive servo problem.* Consider the asymptotically stable, MP plant given by (95). Let r be a harmonic command with amplitude 3 and frequency $\omega = 0.45$ rad/sample, and let $d = v = 0$. We use the FIR target model (20), and set $n_{\mathrm{c}} = 12$ and $R_\theta = 0.5$. Figure 55 shows the command-following performance, with

and without control deadzone. ∎

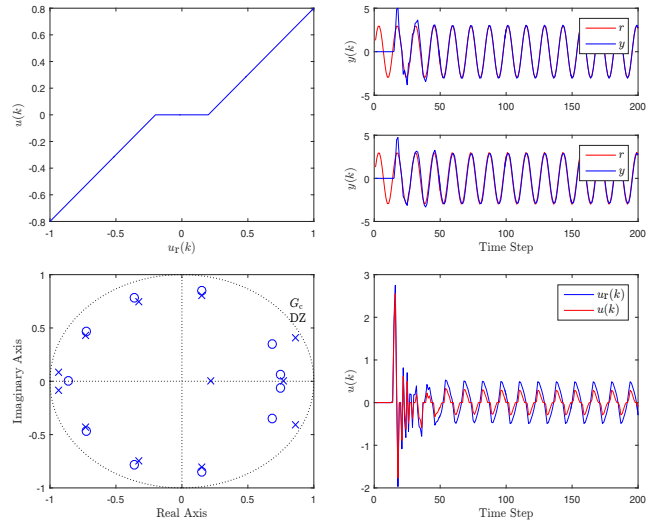Fig. 55. Example 47: Deadzone for the adaptive servo problem. The control u has a deadzone of ± 0.2. RCAC follows the command and develops an internal model of the command, despite the deadzone.

Example 48. *Cubic nonlinearity for the adaptive servo problem.* Consider the asymptotically stable, MP plant given by (95), let r be the harmonic command $r(k) = \cos \omega k$, where $\omega = 0.45$ rad/sample, and let $d = v = 0$. We use the FIR target model (20), and set $n_{\mathrm{c}} = 12$ and $R_\theta = 0.5$. Figure 56 shows the command-following performance, with and without cubic nonlinearity. ∎

IX. CONCLUSIONS

This paper described the rationale and motivation for RCAC, provided a concise description of this adaptive feedback control algorithm, and presented a diverse collection of examples to illustrate some of the features of RCAC. The examples show the effect of the tuning parameters, the modeling requirements of RCAC, and the robustness of RCAC to mismodeled and unmodeled dynamics. Some of these features are well understood based on the current theoretical development of RCAC. Others, however, are empirical, and
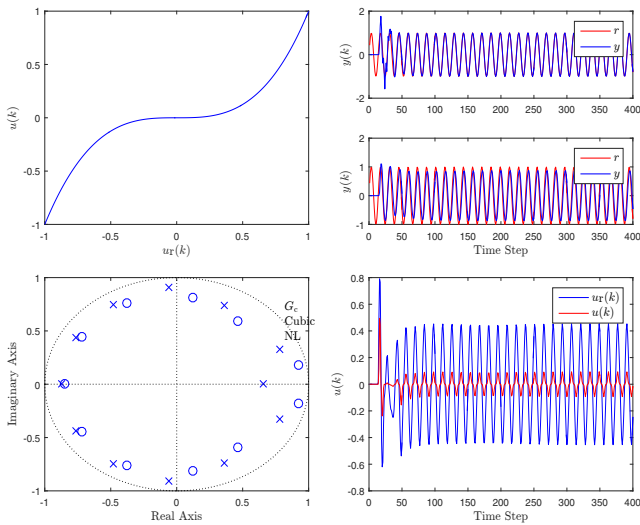
Fig. 56. Example 48: Effect of cubic nonlinearity on command-following performance for (95).

much theoretical work remains to be done to establish a fully developed foundation for this technique. The goal of this paper has thus been to provide a comprehensive tutorial of RCAC as an adaptive control technique with enough detail to convey the potential of this method in diverse applications. RCAC is based on re-optimization of the controller, which is a variation of quadratic optimization that is effective with surprisingly little modeling information. This technique has application beyond adaptive control, for example, in system identification and state estimation. To this extent, RCAC can lead to new algorithms that may be effective for a wide range of problems in systems and control theory.

APPENDIX

It is shown in [20], [48] that the closed-loop poles of high-authority LQG control without sensor noise converge to locations that depend on the zeros of G_{zu} and G_{yw}. Consider the factorizations of the numerators N_{zu} and N_{yw} of G_{zu} and G_{yw}, respectively, given by

$$N_{zu}(\mathbf{q}) = N_{zu,\mathrm{s}}(\mathbf{q})N_{zu,\mathrm{u}}(\mathbf{q}), \qquad (105)$$

$$N_{yw}(\mathbf{q}) = N_{yw,\mathrm{s}}(\mathbf{q})N_{yw,\mathrm{u}}(\mathbf{q}), \qquad (106)$$

where the roots of $N_{zu,\mathrm{s}}(\mathbf{q})$ and $N_{yw,\mathrm{s}}(\mathbf{q})$ are minimum-phase zeros and the roots of $N_{zu,\mathrm{u}}(\mathbf{q})$ and $N_{yw,\mathrm{u}}(\mathbf{q})$ are NMP zeros. Let d_{zu} denote the relative degree of G_{zu} and let d_{yw} denote the relative degree of G_{yw}. Then the closed-loop poles of high-authority LQG control without sensor noise are the roots of

$$\widetilde{D}(\mathbf{q}) = \mathbf{q}^{d_{zu}+d_{yw}} N_{zu,\mathrm{s}}(\mathbf{q})N_{zu,\mathrm{u}}(1/\mathbf{q})N_{yw,\mathrm{s}}(\mathbf{q})N_{yw,\mathrm{u}}(1/\mathbf{q}).$$
$$(107)$$

Note that the zeros of $N_{zu,\mathrm{u}}(1/\mathbf{q})$ are the reflections across the unit circle of the NMP zeros of G_{zu}, that is, reciprocals. For example, if $N_{zu,\mathrm{u}}(\mathbf{q}) = \mathbf{q} - 1.2$, then $N_{zu,\mathrm{u}}(1/\mathbf{q}) = \mathbf{q} - \frac{1}{1.2}$.

Example A1: High-authority LQG control without sensor

noise for a plant with $y \neq z$ and with w not matched with u. Consider the asymptotically stable plant with $y \neq z$, and with w not matched with u, shown in Figure 57. We apply LQG to this plant with zero control cost weighting. The resulting closed-loop pole locations are shown in Figure 57. ∎
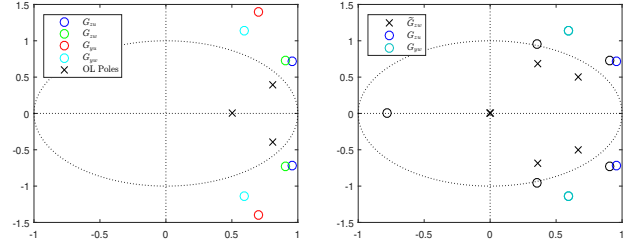

Fig. 57. Example A1: High-authority LQG control without sensor noise for a plant with $y \neq z$ and with w not matched with u. The closed-loop transfer function $\widetilde{G}_{zw}$ has poles at the minimum-phase zeros of G_{zu} and G_{yw} and at the reflections of the NMP zeros of G_{zu} and G_{yw}. Each remaining closed-loop pole is either canceled by a closed-loop zero or is located at zero.

Example A2: High-authority LQG control without sensor noise for a plant with $y = z$ and with w matched with u. Consider the asymptotically stable plant with $y = z$ and with w matched with u, shown in Figure 58. We apply LQG to this plant with zero control cost weighting. The resulting closed-loop pole locations are shown in Figure 58. ∎
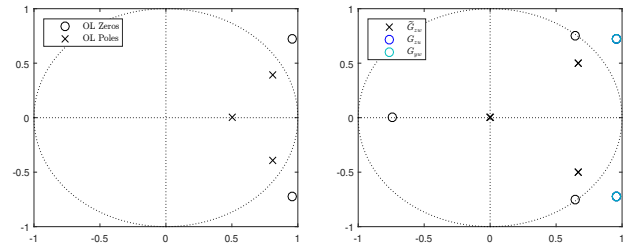

Fig. 58. Example A2: High-authority LQG control without sensor noise for a plant with $y = z$ and with w matched with u. Note that, in this case, the closed-loop transfer function $\widetilde{G}_{zw}$ has double poles at the minimum-phase zeros of the plant and double poles at the reflections of NMP zeros of the plant. Each remaining closed-loop pole is either canceled by a closed-loop zero or is located at zero.

REFERENCES

[1] B. D. O. Anderson and A. Dehghani, "Challenges of Adaptive Control–Past, Permanent and Future," *Ann. Rev. in Contr.*, vol. 32, pp. 123–135, 2008.

[2] G. C. Goodwin, P. J. Ramadge, and P. E. Caines, "Discrete-Time Multi-Variable Adaptive Control," *IEEE Trans. Autom. Control*, vol. 25, pp. 449–456, 1980.

[3] K. J. Åström, "Direct Methods for Nonminimum Phase Systems," in *Proc. Conf. Dec. Contr.*, Albuquerque, NM, December 1980, pp. 611–615.

[4] G. C. Goodwin and K. S. Sin, "Adaptive Control of Nonminimum Phase Systems," *IEEE Trans. Autom. Contr.*, vol. 26, pp. 478–483, 1981.

[5] R. Johansson, "Parametric Models of Linear Multivariable Systems for Adaptive Control," *IEEE Trans. Autom. Contr.*, vol. 32, pp. 303–313, 1987.

[6] L. Praly, S. T. Hung, and D. S. Rhode, "Towards a Direct Adaptive Scheme for a Discrete-Time Control of a Minimum Phase Continuous-Time System," in *Proc. Conf. Dec. Contr.*, Fort Lauderdale, FL, December 1989, pp. 1188–1191.

[7] R. Venugopal, V. G. Rao, and D. S. Bernstein, "Lyapunov-Based Backward-Horizon Discrete-Time Adaptive Control," *Adaptive Contr. Sig. Proc.*, vol. 17, pp. 67–84, 2003.

[8] T. Hayakawa, W. M. Haddad, and A. Leonessa, "A Lyapunov-Based Adaptive Control Framework for Discrete-time Non-linear Systems with Exogenous Disturbances," *Int. J. Control*, vol. 77, pp. 250–263, 2004.

[9] S. Akhtar, R. Venugopal, and D. S. Bernstein, "Logarithmic Lyapunov Functions for Direct Adaptive Stabilization with Normalized Adaptive Laws," *Int. J. Contr.*, vol. 77, pp. 630–638, 2004.

[10] J. B. Hoagg, M. A. Santillo, and D. S. Bernstein, "Discrete-time Adaptive Command Following and Disturbance Rejection with Unknown Exogenous Dynamics," *IEEE Trans. Autom. Contr.*, vol. 53, pp. 912–928, 2008.

[11] C.-C. Cheng and S. H.-S. Fu, "On Trajectory-Dependent Direct Adaptive Control for a Class of Uncertain Linear Discrete-time Systems," *Int. J. Adapt. Contr. Signal Proc.*, vol. 23, pp. 1014–1030, 2009.

[12] C. Li and J. Lam, "Stabilization of Discrete-Time Nonlinear Uncertain Systems by Feedback Based on LS Algorithm," *SIAM J. Contr. Optim.*, vol. 51, pp. 1128–1151, 2013.

[13] M. Yu, J.-X. Xu, and D. Huang, "Discrete-Time Periodic Adaptive Control for Parametric Systems with Non-sector Nonlinearities," *Int. J. Adapt. Contr. Signal Proc.*, vol. 28, pp. 987–1001, 2014.

[14] H. Hjalmarsson, M. Gevers, S. Gunnarsson, and O. Lequin, "Iterative feedback tuning: theory and applications," *IEEE Contr. Sys. Mag.*, vol. 18, no. 4, pp. 26–41, 1998.

[15] D. Bristow, M. Tharayil, and A. G. Alleyne, "A survey of iterative learning control," *IEEE Contr. Sys. Mag.*, vol. 26, no. 3, pp. 96–114, 2006.

[16] R. Venugopal and D. S. Bernstein, "Adaptive Disturbance Rejection Using ARMARKOV System Representations," *IEEE Trans. Contr. Sys. Tech.*, vol. 8, pp. 257–269, 2000.

[17] M. A. Santillo and D. S. Bernstein, "Adaptive Control Based on Retrospective Cost Optimization," *J. Guid. Contr. Dyn.*, vol. 33, pp. 289–304, 2010.

[18] J. B. Hoagg and D. S. Bernstein, "Retrospective Cost Model Reference Adaptive Control for Nonminimum-Phase Systems," *J. Guid. Contr. Dyn.*, vol. 35, pp. 1767–1786, 2012.

[19] E. D. Sumer and D. S. Bernstein, "Robust Sampled-Data Adaptive Control of the Rohrs Counterexamples," in *Proc. Conf. Dec. Contr.*, Maui, HI, December 2012, pp. 7273–7278.

[20] E. D. Sumer, J. B. Hoagg, and D. S. Bernstein, "Broadband Disturbance Rejection Using Retrospective Cost Adaptive Control," in *Proc. Dyn. Sys. Contr. Conf.*, no. DSCC2012-MOVIC2012-8572, Fort Lauderdale, FL, October 2012, pp. 1–10.

[21] J. Yan and D. S. Bernstein, "Minimal Modeling Retrospective Cost Adaptive Control of Uncertain Hammerstein Systems Using Auxiliary Nonlinearities," *Int. J. Contr.*, vol. 87, pp. 483–505, 2014.

[22] E. D. Sumer and D. S. Bernstein, "On the Role of Subspace Zeros in Retrospective Cost Adaptive Control of Nonsquare Plants," *Int. J. Contr.*, vol. 88, pp. 295–323, 2015.

[23] M. Rizzo, M. A. Santillo, A. Padthe, J. B. Hoagg, S. Akhtar, D. S. Bernstein, and K. G. Powell, "CFD-Based Identification for Adaptive Flow Control Using ARMARKOV Disturbance Rejection," in *Proc. Amer. Contr. Conf.*, Minneapolis, MN, June 2006, pp. 3783–3788.

[24] Y.-C. Cho, J. B. Hoagg, D. S. Bernstein, and W. Shyy, "Retrospective Cost Adaptive Flow Control of Low-Reynolds Number Aerodynamics Using a Dielectric Barrier Discharge Actuator," in *Proc. 5th AIAA Flow Contr. Conf.*, Chicago, IL, August 2010, AIAA-2010-4841.

[25] M. Isaacs, J. B. Hoagg, A. V. Morozov, and D. S. Bernstein, "A Numerical Study on Controlling a Nonlinear Multilink Arm Using A Retrospective Cost Model Reference Adaptive Controller," in *Proc. Conf. Dec. Contr.*, Orlando, FL, December 2011, pp. 8008 – 8013.

[26] E. D. Sumer and D. S. Bernstein, "Adaptive Decentralized Noise and Vibration Control with Conflicting Performance Objectives," in *Proc. Dyn. Sys. Contr. Conf.*, no. DSCC2012-MOVIC2012-8580, Fort Lauderdale, FL, October 2012, pp. 1–10.

[27] E. D. Sumer and D. S. Bernstein, "Adaptive Control of Flexible Structures with Uncertain Dynamics and Uncertain Disturbance Spectra," in *Proc. AIAA Guid. Nav. Contr. Conf.*, Minneapolis, MN, August 2012, AIAA-2012-4437-323.

[28] A. K. Padthe, P. P. Friedmann, and D. S. Bernstein, "Retrospective Cost Adaptive Control for Helicopter Vibration Reduction," in *Proc. AHS 69th Annual Forum*, Phoenix, AZ, May 2013, AHS2013-000179.

[29] J. Yan, A. M. D'Amato, K. Butts, I. Kolmanovsky, and D. S. Bernstein, "Adaptive Control of the Air Flow System in a Diesel Engine," in *Proc. Dyn. Sys. Contr. Conf.*, no. DSCC2012-MOVIC2012-8597, Fort Lauderdale, FL, October 2012, pp. 1–9.

[30] M. J. Yu, Y. Rahman, E. M. Atkins, I. Kolmanovsky, and D. S. Bernstein, "Minimal Modeling Adaptive Control of the NASA Generic Transport Model with Unknown Control-Surface Faults," in *Proc. AIAA Guid. Nav. Contr. Conf.*, Boston, MA, August 2013, AIAA-2013-4693.

[31] F. Sobolic and D. S. Bernstein, "Aerodynamic-free adaptive control of the NASA generic transport model," in *Proc. AIAA Guid. Nav. Contr. Conf.*, Boston, MA, August 2013, AIAA-2013-4999.

[32] M. J. Yu, J. Zhong, E. M. Atkins, I. V. Kolmanovsky, and D. S. Bernstein, "Trim-commanded adaptive control for waypoint-defined trajectory following," in *Proc. AIAA Guid. Nav. Contr. Conf.*, Boston, MA, August 2013, AIAA-2013-4999.

[33] A. Ansari and D. S. Bernstein, "Adaptive Control of an Aircraft with Uncertain Nonminimum-Phase Dynamics," in *Proc. Amer. Contr. Conf.*, Chicago, IL, July 2015, pp. 844–849.

[34] M. Camblor, G. Cruz, S. Esteban, F. A. Leve, and D. S. Bernstein, "Retrospective Cost Adaptive Spacecraft Attitude Control Using Control Moment Gyros," in *Proc. Amer. Contr. Conf.*, Portland, OR, June 2014, pp. 2492–2497.

[35] S. Dai, T. Lee, and D. S. Bernstein, "Adaptive Control of a Quadrotor UAV Transporting a Cable-Suspended Load with Unknown Mass," in *Proc. Conf. Dec. Contr.*, Los Angeles, CA, December 2014, pp. 6149–6154.

[36] F. Sobolic and D. S. Bernstein, "An Inner-Loop/Outer-Loop Architecture for an Adaptive Missile Autopilot," in *Proc. Amer. Contr. Conf.*, Chicago, IL, July 2015, pp. 850–855.

[37] A. Goel, A. Xie, K. Duraisamy, and D. S. Bernstein, "Retrospective Cost Adaptive Thrust Control of a 1D Scramjet with Mach Number Disturbance," in *Proc. Amer. Contr. Conf.*, Chicago, IL, July 2015, pp. 5551–5556.

[38] M. A. Janaideh and D. S. Bernstein, "Adaptive Control of Hammerstein Systems with Unknown Prandtl-Ishlinskii Hysteresis," *Proc. IMechE Part 1: J. Sys. Contr. Eng.*, pp. 1–9, 2014.

[39] H. Sane and D. S. Bernstein, "Active Noise Control Using an Acoustic Servovalve," in *Proc. Amer. Contr. Conf.*, Philadelphia, PA, June 1998, pp. 2621–2625.

[40] H. Sane, R. Venugopal, and D. S. Bernstein, "Disturbance Rejection Using Self-Tuning ARMARKOV Adaptive Control with Simultaneous Identification," *IEEE Trans. Contr. Sys. Tech.*, vol. 19, pp. 101–106, 2001.

[41] S. L. Lacy, R. Venugopal, and D. S. Bernstein, "ARMARKOV Adaptive Control of Self-Excited Oscillations of a Ducted Flame," in *Proc. Conf. Dec. Contr.*, Tampa, FL, December 1998, pp. 4527–4528.

[42] B. L. Pence, M. A. Santillo, and D. S. Bernstein, "Markov-Parameter-Based Adaptive Control of 3-Axis Angular Velocity in a 6DOF Stewart Platform," in *Proc. Amer. Contr. Conf.*, Seattle, WA, June 2008, pp. 4767–4772.

[43] A. V. Roup and D. S. Bernstein, "Adaptive Stabilization of a Class of Nonlinear Systems with Nonparametric Uncertainty," *IEEE Trans. Autom. Contr.*, vol. 46, no. 11, pp. 1821–1825, 2001.

[44] M. Vidyasagar, *Control System Synthesis: A Factorization Approach*. MIT Press, 1985.

[45] A. R. Teel, "Global Stabilization and Restricted Tracking for Multiple Integrators with Bounded Controls," *Systems & Control Letters*, vol. 18, no. 3, pp. 165–171, 1992.

[46] T. Lauvdal, R. M. Murray, and T. I. Fossen, "Stabilization of Integrator Chains in the Presence of Magnitude and Rate Saturations: a Gain Scheduling Approach," in *Proc. Conf. Dec. Contr.*, San Diego, CA, December 1997, pp. 4004–4005.

[47] B. J. Coffer, J. B. Hoagg, and D. S. Bernstein, "Cumulative Retrospective Cost Adaptive Control of Systems with Amplitude and Rate Saturation," in *Proc. Amer. Contr. Conf.*, San Francisco, CA, July 2011, pp. 2344–2349.

[48] H. Kwakernaak and R. Sivan, *Linear Optimal Control Systems*. Wiley, 1972.